PHYSICAL REVIEW D **93,** 055018 (2016)

Role of the 'N' in the natural NMSSM for the LHC

Jong Soo Kim[*]
Instituto de Fisica Teorica UAM/CSIC, 28049 Madrid, Spain

Daniel Schmeier[†]
Physikalisches Institut and Bethe Center for Theoretical Physics, University of Bonn, 53115 Bonn, Germany

Jamie Tattersall[‡]
Institut für Theoretische Teilchenphysik und Kosmologie, RWTH Aachen, 52056 Aachen, Germany
(Received 9 November 2015; published 11 March 2016)

In this work, we present mass limits on gluinos and stops in a *natural* next-to-minimal supersymmetric Standard Model with a singlino as the lightest supersymmetric particle. Motivated by naturalness, we consider spectra with light Higgsinos, sub-TeV third generation sparticles and gluinos well below the multi-TeV regime while the electroweak gauginos, the sleptons and the first and second generation squarks are decoupled. We check that our natural supersymmetry spectra satisfy all electroweak precision observables and flavor measurements as well as theoretical constraints. By reinterpreting the results from the 8 TeV ATLAS supersymmetry searches we present the 95% C.L. exclusion limits on the model. The results show that the presence of a singlino lightest supersymmetric particle can lengthen decay chains and soften the final state particle energies. While this does reduce the strength of the bounds in some areas of parameter space, the LHC still displays good sensitivity to the model.

DOI: 10.1103/PhysRevD.93.055018

I. INTRODUCTION

The discovery of a Higgs boson at the Large Hadron Collider in 2012 [1–3] was a triumph for experimental particle physics. Its measured mass of ≈125 GeV fits perfectly into the framework of the Standard Model (SM), which required—and hence predicted—a scalar particle with mass of the order ≤2 TeV from unitarity constraints [4]. Moreover, the observed Higgs mass falls into the narrow mass window $m_h = 96^{+31}_{-24}$ GeV predicted in global fits of the SM model to precision electroweak observables [5]. However, this theory suffers from a well-known hierarchy problem due to the quadratic sensitivity of the Higgs mass to new physical scales. Supersymmetry (SUSY) [6–9] is able to ameliorate this problem and to stabilize the Higgs mass at the electroweak scale by canceling the quadratic divergences. However, the minimal incorporation into the Standard Model, called the minimal supersymmetric Standard Model (MSSM), leads to the prediction that the CP-even Higgs should be lighter than the Z boson at tree level. Under the assumption that the LHC has measured the lightest supersymmetric Higgs boson, we thus require significant radiative corrections in order to raise the mass to the experimentally measured value. These corrections are often provided by the supersymmetric partners of the top quark, called stop squarks, since their large Yukawa couplings dictate that they provide the leading one-loop correction.

In the MSSM, the Higgs is expected to have a mass between 113 and 135 GeV [10]. However, the problem is that these corrections only reproduce the correct Higgs mass when both stop masses have very large masses for negligible mixing in the stop sector, or the trilinear A_t term is very large with at least one heavy stop (e.g. [11]). This is an issue since a large separation between the electroweak and SUSY breaking scale introduces the *little hierarchy problem* [12]. Thus, in this case the model is deemed to be "unnatural" since fine-tuned cancellations are still required. To confront this issue in the MSSM, extended models that already predict a heavier Higgs mass at the tree level have become popular. The simplest example of such a model is known as the next-to-minimal supersymmetric Standard Model (NMSSM) where an extra gauge singlet chiral superfield is added to the spectrum [13]. Since the singlet superfield couples both to the up- and the down-type Higgs superfield, the singlet scalar components contribute to the Higgs potential and can thus raise the tree-level Higgs mass, reducing the need for heavy stops.

In addition, the only dimensionful SUSY conserving parameter, μ, of the MSSM can be dynamically generated in the NMSSM by a nonvanishing vacuum expectation value s of the extra singlet scalar. To get a phenomenologically acceptable scenario of electroweak symmetry breaking, $|\mu|$ should lie within M_Z and M_{SUSY}, the scale

[*]jong.kim@csic.es
[†]daschm@th.physik.uni-bonn.de
[‡]tattersall@physik.rwth-aachen.de

where supersymmetry is broken. In the MSSM, the scale of μ is in principle arbitrary and no theoretical reasoning binds it to low scales, which leads to the so-called μ problem [14]. In the NMSSM, however, the effective μ parameter is determined by the scale of the vacuum expectation value (vev) s, which is automatically of the right order.

The large Higgs mass is not the only experimental evidence from the LHC that puts the idea of SUSY solving the hierarchy problem under strain. The fact that no SUSY particles have yet been seen pushes the limits on SUSY gluons, called gluinos, and SUSY quarks, called squarks, to masses ≥ 1.5 TeV (see e.g. [15]) that would already be deemed unnatural in constrained models like the constrained minimal supersymmetric Standard Model. These results have motivated a deeper study of exactly which pieces of the SUSY spectrum are required to be light for a theory to be considered natural [16]. Firstly, since the singlet itself now generates the μ parameter that sets the Higgs(ino) masses, all of these particles, including the fermionic partner of the singlet (singlino), can be expected to have masses of the same order. Furthermore, the dominant one-loop corrections to the Higgs sector come from the stops and consequently these cannot be too heavy. Also, since the gluino yields a sizeable correction to the stop masses at one loop, we also have another, looser constraint on the mass of this particle for the same reason. Finally due to the weak isospin symmetry, the partners of the left handed bottom quarks (sbottoms), must have a mass similar to that of the left handed stops.

Consequently we are drawn to a SUSY spectrum with light singlinos and Higgsinos, stops and sbottoms that may be a little more massive and a gluino that can be heavier still. Since none of the other SUSY partners are required by naturalness principles to be light enough to be seen at the LHC, we simply decouple these from our spectrum in this study.

In the context of the MSSM, naturalness is now used as a guiding principle for many LHC searches for gluinos, stops, sbottoms. These studies set bounds on the gluino of $m_{\tilde{g}} \geq 1150$ GeV in the case of a light ($m_{\tilde{\chi}_1^0} \lesssim 100$ GeV) lightest supersymmetric particle (LSP), but this can be reduced to $m_{\tilde{g}} \geq 500$ GeV in the limit that the gluino becomes degenerate with the LSP [15,17–21]. For stops, the bounds can reach up to $m_{\tilde{t}} \geq 700$ GeV, if the dominate decay mode is $\tilde{t} \to t\tilde{\chi}_1^0$, and $m_{\tilde{t}} \gtrsim 600$ GeV for $\tilde{t} \to b\tilde{\chi}_1^+$. Again, if the spectrum is compressed, the bounds weaken significantly and the limit is only $m_{\tilde{t}} \gtrsim 255$ GeV for $m_{\tilde{t}_1} - m_{\tilde{\chi}_1^0} \approx m_b$ [22]. In addition there are regions of parameter space ($m_{\tilde{t}} \sim m_t + m_{\tilde{\chi}_1^0}$) where no limit can be set at all since the kinematics very closely resemble the SM $t\bar{t}$ background but with a substantially smaller production cross section [19,23–26]. Sbottom limits are similar to those of stops (up to $m_{\tilde{b}} \geq 650$ GeV for light $\tilde{\chi}_1^0$ and $m_{\tilde{b}} \geq 250$ GeV in compressed regions) but are more robust and do not contain holes as we move across the mass plane [23,27–29].

Since the LHC direct production constraints still allow for relatively light gluinos and have no model independent limit on the stop mass, the question of naturalness is driven by the Higgs mass in the MSSM. In the NMSSM however, the reduced need for heavy stops to contribute to the Higgs means that the direct production constraints become far more relevant. In addition, the limits can be expected to be different since a light singlino will be present in the spectrum. However, as the singlino does not couple directly to the squarks the state does not normally contribute to LHC phenomenology unless it is the lightest particle in the spectrum (LSP). The effect of a singlino LSP has now been examined in a number of studies and it has been claimed that it generally weakens the LHC limits since the longer decay chains soften the p_T spectra and reduces the E_T^{miss} [30–33]. Other studies have also looked at purely Higgsino-singlino spectra [34,35], direct stop [36,37] or gluino [38] production and the possibility that the singlino may be light [39–44]. A comprehensive list of the expected signatures of the NMSSM is given in [45] while [46] has explored possible methods to distinguish the NMSSM from the more commonly discussed MSSM.

In this study we wish to explore in detail the claim that a singlino LSP generally weakens the LHC bounds. As stated above this is expected and seen [30,31] because the longer decay chain produce softer particles for similar LSP masses. However if we examine the particles produced in the extra NMSSM decay we see that this may not always be true. In particular the decays that may occur are $\tilde{\chi}_2^0 \to \tilde{\chi}_1^0 X^0$ where X^0 is either a Z^0 or Higgs and $\tilde{\chi}_2^\pm \to \tilde{\chi}_1^0 X^\pm$ where $X\pm$ is either a $W^\pm$ or a charged Higgs. In the case of $W^\pm$ or Z^0 production we can expect increased production of leptons over the MSSM that may improve the bounds but the branching-ratio suppression makes it unlikely that this will result in a large change. However a bigger difference can be expected when a Higgs is produced that will decay to a $b\bar{b}$ final state. If the mass splitting $m_{\tilde{\chi}_2^0} - m_{\tilde{\chi}_1^0} > m_h$, then this decay dominates in a large portion of the natural NMSSM parameter space. The reason that this final state can be so important for LHC phenomenology is that many SUSY searches use b tags as a way to suppress the SM background (e.g. [47–50]) and some even search for the presence of on-shell Higgs bosons e.g ([51–55]). Both of these strategies give the possibility that the natural NMSSM may be even more constrained than the MSSM.

In order to fully test the effect of the additional b quarks we require many LHC searches to be simultaneously checked. For this reason we use the CheckMATE tool [56] which now contains over 40 analyses implemented via AnalysisManager [57]. In addition, we also test various theoretical and experimental constraints via NMSSMTools [58–62], HiggsSignals [63] and HiggsBounds [64].

We begin the paper by describing the Lagrangian of the natural NMSSM in Sec. II and the spectrum that we decide to investigate along with the LHC signatures this will lead to. In Sec. III we describe exactly how the model parameters are chosen and the experimental and theoretical constraints that are applied. Here we also introduce how we perform the LHC phenomenology in this paper. Section IV displays the results of our study, concentrating on the LHC bounds now present on the natural NMSSM. Finally in Sec. V we conclude.

II. A PHENOMENOLOGICALLY NATURAL NMSSM

A. Lagrangian, masses and parameters

In the following we present the Lagrangian formulation of our model, the resulting mass matrices and the features that motivate our spectra. Most definitions and relations are taken from [13] and we refer readers to check this source and references therein for more information.

The NMSSM extends the well-known MSSM by an additional chiral superfield $\hat{S}$ which is uncharged under the Standard Model gauge groups. In this work we consider a simplified, natural version of a $\mathbb{Z}_3$-invariant NMSSM. Here, only terms involving exactly three fields are allowed to appear in the superpotential, for reasons explained below. Furthermore, only the scalar partners of the gluon and the third generation quarks plus the fermionic components of the three Higgs superfields $\hat{H}_u$, $\hat{H}_d$ and $\hat{S}$ are assumed to be phenomenologically observable among all supersymmetric particles. This setup can be described by the following superpotential:

$$\mathcal{W} = h_t(\hat{Q}_3 \cdot \hat{H}_u)\hat{t}_R^c + h_b(\hat{Q}_3 \cdot \hat{H}_d)\hat{b}_R^c + \lambda(\hat{H}_u \cdot \hat{H}_d)\hat{S} + \frac{\kappa}{3}\hat{S}^3, \tag{1}$$

where the $\cdot$ symbol denotes the usual SU(2) invariant antisymmetric product of the respective isospin doublets $\hat{H}_u \equiv (\hat{H}_u^+, \hat{H}_u^0), \hat{H}_d \equiv (\hat{H}_d^0, \hat{H}_d^-)$ and $\hat{Q}_3 \equiv (\hat{t}_L, \hat{b}_L)$. Here, h_t and h_b are the dimensionful Yukawa couplings, while λ and κ correspond to dimensionless Yukawas. Note that the assumed additional $\mathbb{Z}_3$ symmetry prohibits the term $\mu(\hat{H}_u \cdot \hat{H}_d)$ usually present in the MSSM and hence provides a superpotential without any dimensionful parameters. A vev of the scalar singlet $\langle S \rangle \equiv s$ of electroweak scale order reintroduces this term after expanding the scalar field S around its minimum and thus generates an effective μ-term $\lambda s(H_u \cdot H_d) \equiv \mu_{\text{eff}}(H_u \cdot H_d)$ of naturally the correct scale, evading the known μ problem of the MSSM:

In addition to the terms derived from this superpotential, the following dimensionful "soft" parameters have to be added to the Lagrangian of the theory:

$$-\mathcal{L}_{\text{soft}}^{\text{mass}} = m_{H_u}^2|H_u|^2 + m_{H_d}^2|H_d|^2 + m_S^2|S|^2 + \frac{1}{2}M_3\tilde{g}\tilde{g} + m_{\tilde{Q}_3}^2|\tilde{Q}_3|^2 + m_{\tilde{U}_3}^2|\tilde{t}_R|^2 + m_{\tilde{D}_3}^2|\tilde{b}_R|^2, \tag{2}$$

$$-\mathcal{L}_{\text{soft}}^{\text{trilinear}} = h_t A_t(\tilde{Q}_3 \cdot H_u)\tilde{t}_R^* + h_b A_b(\tilde{Q}_3 \cdot H_d)\tilde{b}_R^* + \lambda A_\lambda(H_u \cdot H_d)S + \frac{\kappa}{3}A_\kappa S^3 + \text{H.c.} \tag{3}$$

Here, $\tilde{g}$ denotes the gluino, i.e. the fermionic part of the vector superfield associated to the SU(3) gauge group. All other field names denote the scalar component of the respective chiral superfield in the superpotential. We assume all couplings to be real valued to simplify the discussion.

The other SUSY particles, namely the squarks of the first two generations, the sleptons as well as the $\text{SU}(2) \times \text{U}(1)$ gauginos are assumed to be decoupled from the experimentally accessible spectrum as explained in Sec. II B. Consequently they are not listed here.

Adding $\mathcal{L}_{\text{soft}}$ to the supersymmetric F- and D-terms yields the full scalar potential from which three minimization conditions for the nonvanishing singlet vevs and the doublet vevs $\langle H_{u/d} \rangle \equiv v_{u/d}$ can be derived:

$$m_{H_u}^2 + \mu_{\text{eff}}^2 + \lambda^2 v_d^2 + \frac{(g_1^2 + g_2^2)}{4(v_u^2 - v_d^2)} = \mu_{\text{eff}} B_{\text{eff}} \cot\beta, \tag{4}$$

$$m_{H_d}^2 + \mu_{\text{eff}}^2 + \lambda^2 v_u^2 + \frac{(g_1^2 + g_2^2)}{4(v_d^2 - v_u^2)} = \mu_{\text{eff}} B_{\text{eff}} \tan\beta, \tag{5}$$

$$m_S^2 + \kappa s(A_\kappa + 2\kappa s) + \lambda^2 v^2 - \lambda\kappa v_u v_d = \lambda \frac{v_u v_d}{s} B_{\text{eff}} \tag{6}$$

with $B_{\text{eff}} \equiv (A_\lambda + \kappa s)$, $v^2 \equiv v_u^2 + v_d^2$. The first two of these can be reformulated as follows:

$$\frac{M_Z^2}{2} = \frac{2}{\tan\beta^2 - 1}(m_{H_d}^2 - \tan\beta^2 m_{H_u}^2) - \mu_{\text{eff}}^2, \tag{7}$$

$$\frac{\sin 2\beta}{2} = \frac{\mu_{\text{eff}} B_{\text{eff}}}{m_{H_u}^2 + m_{H_d}^2 + 2\mu_{\text{eff}}^2 + \lambda^2 v^2}. \tag{8}$$

Here we have used the fact that $M_Z^2 = v^2(g_1^2 + g_2^2)/2$ is fixed by the known mass of the Z boson. The above equations allow one to choose the parameters in the set $\{\lambda, \kappa, A_\lambda, A_\kappa, \mu_{\text{eff}}, \tan\beta \equiv v_u/v_d\}$ to be independent, where μ_{eff}, $\tan\beta$ and the known Standard Model parameter M_Z replace the Lagrangian parameters $m_{H_u}^2$, $m_{H_d}^2$ and m_S^2. After expanding H_u, H_d and S around their minima, one gets the following symmetric mass matrix for their CP-even components $\{h_u, h_d, h_s\}$ at tree level:

$$\mathcal{M}^2_{\text{scalar}} = \begin{pmatrix} g^2 v_d^2 + \mu_{\text{eff}} B_{\text{eff}} \tan\beta & (2\lambda^2 - g^2) v_u v_d - \mu_{\text{eff}} B_{\text{eff}} & \lambda(2\mu_{\text{eff}} v_d - (B_{\text{eff}} + \kappa s) v_u) \\ \cdots & g^2 v_u^2 + \mu_{\text{eff}} B_{\text{eff}} \cot\beta & \lambda(2\mu_{\text{eff}} v_u - (B_{\text{eff}} + \kappa s) v_d) \\ \cdots & \cdots & \lambda A_\lambda v_u v_d / s + \kappa s A_\kappa + 4\kappa^2 s^2 \end{pmatrix}, \tag{9}$$

with $g^2 \equiv M_Z/(v_u^2 + v_d^2)$ given by the Standard Model gauge sector. We call the diagonalized mass eigenstates h, H and H_3 which have increasing mass from left to right.

Similarly, the matrix of the respective CP-odd components $\{a_u, a_d, a_s\}$ reads

$$\mathcal{M}^2_{\text{pseudoscalar}} = \begin{pmatrix} \mu_{\text{eff}} B_{\text{eff}} \tan\beta & \mu_{\text{eff}} B_{\text{eff}} & \lambda v_u (A_\lambda - 2\kappa s) \\ \cdots & \mu_{\text{eff}} B_{\text{eff}} \cot\beta & \lambda v_d (A_\lambda - 2\kappa s) \\ \cdots & \cdots & \lambda(A_\lambda + 4\kappa s) v_u v_d / s - 3\kappa A_\kappa s \end{pmatrix}, \tag{10}$$

which yields one massless Goldstone mode and two CP-odd mass eigenstates A_1 and A_2.

Finally, the charged components $\{h_u^+, h_d^{-*}\}$ have the mass matrix:

$$\mathcal{M}^2_{\pm} = m^2_{\pm} \cdot \begin{pmatrix} \cot\beta & 1 \\ 1 & \tan\beta \end{pmatrix} \tag{11}$$

$$\text{with} \quad m^2_{\pm} \equiv \mu_{\text{eff}}(A_\lambda + \kappa s) + v_u v_d (g_2^2/2 - \lambda^2), \tag{12}$$

resulting in one massless Goldstone mode and one massive charged Higgs boson $H^\pm$.

Since we consider the wino and bino to be decoupled at a heavier mass scale, we can simplify the neutralino sector to only contain the three neutral fermionic partners of the fields, $\tilde{h}_u^0$, $\tilde{h}_d^0$ and $\tilde{s}$. These mix to three physical neutralinos $\tilde{\chi}^0_{1,2,3}$ after diagonalizing the matrix

$$\mathcal{M}_{\text{neutralinos}} = \begin{pmatrix} 0 & -\mu_{\text{eff}} & -\lambda v_u \\ \cdots & 0 & -\lambda v_d \\ \cdots & \cdots & 2\kappa s \end{pmatrix}. \tag{13}$$

The two charged Higgsino components combine to a single Dirac chargino $\tilde{\chi}_1^\pm$ with mass term $\frac{1}{2}\mu_{\text{eff}} \tilde{h}_u^+ \tilde{h}_d^- + \text{H.c.}$.

In the following, we will use the collective term "Higgsino" ($\tilde{h}$) for the two Higgsino-like neutralinos and the chargino. Furthermore, for the sake of simplicity, we will use "electroweakino" ($\tilde{\chi}$) collectively for all three neutralinos and the chargino, even though strictly speaking $\tilde{s}$ does not have any electroweak charge.

The stop and sbottom tree-level mass matrices in the bases $(\tilde{t}_R, \tilde{t}_L)$ and $(\tilde{b}_R, \tilde{b}_L)$ read

$$\mathcal{M}^2_{\text{stops}} = \begin{pmatrix} m^2_{U_3} + h_t^2 v_u^2 - (v_u^2 - v_d^2) g_1^2/3 & h_t v_u (A_t - \mu_{\text{eff}} \cot\beta) \\ \cdots & m^2_{Q_3} + h_t^2 v_u^2 + (v_u^2 - v_d^2)(g_1^2/12 - g_2^2/4) \end{pmatrix}, \tag{14}$$

$$\mathcal{M}^2_{\text{sbottoms}} = \begin{pmatrix} m^2_{D_3} + h_b^2 v_d^2 - (v_u^2 - v_d^2) g_1^2/6 & h_b v_d (A_b - \mu_{\text{eff}} \tan\beta) \\ \cdots & m^2_{Q_3} + h_b^2 v_d^2 + (v_u^2 - v_d^2)(g_1^2/12 + g_2^2/4) \end{pmatrix}, \tag{15}$$

with eigenstates $\tilde{t}_{1/2}, \tilde{b}_{1/2}$.

Even though we have not shown the full next-to-leading order corrections to these tree-level masses, it can be understood that the whole model is fixed by Standard Model parameters plus the set $\{\lambda, \kappa, A_\lambda, A_\kappa, \mu_{\text{eff}}, \tan\beta, m^2_{Q_3}, m^2_{U_3}, m^2_{D_3}, A_t, A_b, M_3\}$.

B. Natural spectrum

Naturalness comes into play in the context of Eq. (7). For a model to be natural all of the individual terms should be of order M_Z^2 and no fine-tuned cancellations should be present. In contrast to the μ parameter in the MSSM, which is a free parameter of the superpotential without any *a priori* relation to the electroweak scale, the μ_{eff} parameter in the NMSSM is itself induced by electroweak symmetry breaking and the vacuum expectation value of S. Thus, it is naturally of right order and determines the expected mass scale of the Higgsinos which are mainly determined by μ_{eff}, see Eq. (13) and below. In the limit of vanishing mixing, the tree-level singlino mass reads $\kappa s = \mu_{\text{eff}}(\kappa/\lambda) \lesssim \mu_{\text{eff}}$, where we have used that the stability of the $s \neq 0$ vacuum usually requires $\kappa/\lambda < 1$ [65]. We therefore expect a singlino that is lighter than the Higgsinos in a natural setup.

This tree-level relation is affected by loop corrections to the respective parameters. As an example, the large Yukawa coupling to the stops and their $\mathcal{O}(\alpha_s)$ correction from gluino loops induces a sizeable effect on $m^2_{H_u}$ in Eq. (7) while running from the SUSY breaking scale Λ_S down to the TeV scale. In the leading log approximation [16], these corrections read

$$\Delta m^2_{H_u}|_{\tilde{t}} \approx -\frac{3y_t^2}{8\pi^2}(m^2_{Q_3} + m^2_{U_3} + |A_t|^2)\ln\left(\frac{\Lambda_S}{\text{TeV}}\right), \quad (16)$$

$$\Delta m^2_{H_u}|_{\tilde{g}} \approx -\frac{2y_t^2}{\pi^3}\alpha_s|M_3|^2\ln\left(\frac{\Lambda_S}{\text{TeV}}\right). \quad (17)$$

Naturalness requires these corrections to be moderately small which translates into mass bounds $m_{\tilde{t}} \lesssim m_{\tilde{g}} \lesssim \mathcal{O}(1\ \text{TeV})$. Note that the naturalness bound on $m^2_{Q_3}$ also sets the scale of the $\tilde{b}_L$-like scalars, as they lie in the same $\text{SU}(2)_L$ doublet as the $\tilde{t}_L$ field. Though no equivalent naturalness constraint applies to the $\tilde{b}_R$ scalar, we assume that there is no *a priori* reason why the SUSY breaking mechanism should induce large splittings $m^2_{U_3} - m^2_{D_3}$ or $A_t - A_b$ and thus we assume the soft breaking parameters to be degenerate (see Sec. III). The appearance of a second light sbottom, however, does not affect the collider results significantly.

Parameters related to the $\text{SU}(2) \times \text{U}(1)$ gauginos and the squarks of the first two generations have negligible effect on the parameters in Eq. (7) and thus are not constrained by naturalness arguments. They can therefore safely be set to experimentally inaccessible scales while keeping the electroweak breaking scale small.

Note that the above consideration of naturalness is only performed on the qualitative level and solely serves as a motivation for the hierarchies and mass scales of our following collider study. More quantitative analyses in terms of so-called *fine tuning* are possible but require a more specific formulation of the decoupled supersymmetric sector to get a valid dependence of low-scale observables on independent high-scale parameters (see e.g. [66]).

While trying to keep the parameters natural, our model should still not violate experimental observation, i.e. a Standard-Model-like scalar boson with mass of order 125 GeV should emerge. In the limit where the lightest CP-odd Higgs boson decouples ($M_A \equiv 2\mu_{\text{eff}}(A_\lambda + \kappa s)/\sin 2\beta \to \infty$), the lightest SM-like eigenvalue of Eq. (9) reproduces the well-known MSSM result for $\lambda = 0$

$$m^2_{h,\text{tree}}(\lambda = 0) \approx M_Z^2 \cos^2 2\beta \quad (18)$$

which requires large radiative corrections from the third generation squark sector

$$\Delta m^2_{h,\text{loop}} = \frac{3m_t^4}{4\pi^2 v^2}\left(\ln\left(\frac{M_{\tilde{q}3}}{m_t^2}\right) + \frac{A_t^2}{M^2_{\tilde{q}3}}\left(1 - \frac{A_t^2}{12M^2_{\tilde{q}3}}\right)\right) \quad (19)$$

in order to be raised to the experimental value. Here we assume degenerate soft breaking stop masses $M^2_{\tilde{q}3} \equiv m^2_{Q_3} = m^2_{U_3} \gg m_t^2$. In the NMSSM however, an additional F-term contribution is present that induces extra mixing between H_u and H_d states in the Lagrangian. This term adds a further tree-level correction to the lightest Higgs state,[1]

$$\Delta m^2_{h,\text{mix}} \approx \lambda^2 v^2 \sin^2 2\beta \quad (20)$$

which for sufficiently well-chosen parameters, i.e. large λ and small $\tan\beta$, can render the need for heavy stops obsolete, making it easier to acquire a natural spectrum as explained above.

The benchmark spectra we are going to consider in the upcoming analysis are sketched in Fig. 1. We distinguish two main limits of the NMSSN, steered by the size of the dimensionless coupling parameter λ:

large $\lambda \equiv \lambda_L$ When the coupling λ is large, Eq. (20) suggests that we can reach a large enough Higgs mass if $\sin 2\beta$ is large. In our analysis we choose ($\lambda = 0.7$, $\tan\beta = 2$), with the value for λ chosen at the maximum possible value which does not run into Landau poles at higher scales. In this setup, no large radiative corrections are required and as such it is expected that one can keep both stops (and the respective sbottoms) rather light while still being able to reach the correct Higgs mass. As a consequence all third generation scalars may be kinematically accessible at the LHC. The neutralinos can mix largely in this scenario and direct decays of colored scalars into singlets and singlinos are possible [67].

small $\lambda \equiv \lambda_S$ In case of a very small λ, the Higgs mass is very MSSM-like. To maximize the tree-level value one needs a larger $\tan\beta$, which is why we define this point via ($\lambda = 0.01$, $\tan\beta = 15$). Large radiative corrections are needed, which asks for at least one heavy stop. The sparticles of the MSSM sector decouple from the singlet states and experimentally, the only difference between the MSSM and the NMSSM would be sparticle decays into the singlino LSP. For very small λ, the scalar vev s must be large in order to have a sufficiently large μ-term. This generally translates into $s \gg v_u, v_d$. Contrarily to the previous case, this scenario will come along with a rather split sector of third generation squarks, mostly degenerate

[1]We note that Eq. (20) is a very crude approximation to illustrate the motivation for certain values of λ and $\tan\beta$. The full mixing correction term depends nontrivially on the other NMSSM parameters $\kappa, A_\lambda, A_\kappa$ depending on their relative sizes, see e.g. [13].

Higgsinos and a mostly decoupled singlino and a singlet scalar sector.

In both scenarios, to avoid having a LSP-like chargino we always require the singlino to be lighter than the Higgsinos. Furthermore, we always require the gluino to be heavier than the stops since the limits on the gluino mass are in general significantly more stringent (compare e.g. [15] vs [23]). Therefore we expect the most "natural" scenarios to occur when the stops are lighter.

While the relative hierarchy between stops/sbottoms and the Higgsinos is not fixed by our setup, we will nevertheless find that it is often as depicted in Fig. 1.

C. Signatures of interest

The spectrum described in the previous section leads to interesting signatures for the LHC: due to the light $\tilde{t}$ and $\tilde{b}$ scalars we expect final states with many t and b quarks. The hadronized jets originating from b quarks have a high probability of being correctly tagged as so-called b jets and many analyses from both ATLAS and CMS have been designed to specifically tag final states with these objects, see Sec. III B. In the following we only focus on final states with these objects and neglect other signatures:

In this work, we consider third generation squark and gluino hadroproduction via the strong interaction. In general, the gluon fusion diagrams will be the dominant production channel for not too heavy gluino and third generation scalar masses and the cross section is only determined by the respective mass and spin of the respective final state sparticle at leading order,

$$pp \to \tilde{g}\tilde{g}, \qquad \tilde{t}_i\tilde{t}_i^*, \qquad \tilde{b}_i\tilde{b}_i^* \qquad i \in \{1,2\}.$$

Here, we have omitted the production of electroweakino pairs since the cross section is negligible compared to the production of colored sparticles unless the Higgsino and the singlino are the only kinematically accessible sparticles at the LHC [34,35]—a scenario we are not going to assume. In addition, we have not considered compressed spectra where a hard initial state radiation jet has to be taken into account.

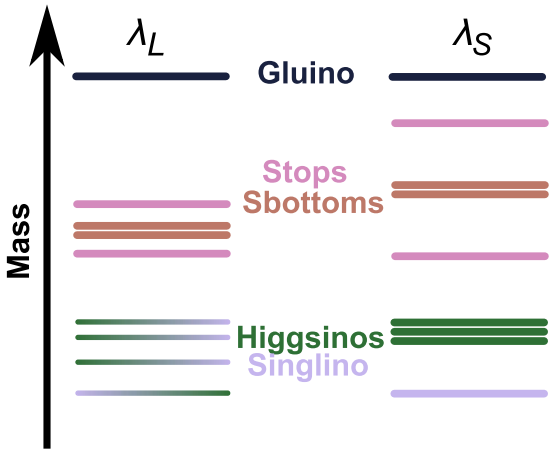

FIG. 1. Schematical setups of the considered benchmark models λ_S and λ_L, their hierarchies and the respective expected mass splittings.

Let us now turn to the discussion of the decay modes. The decay chains can be very complicated in natural SUSY and typically depends on the details of the mass spectrum and the mixing angles. Since we define that the gluino is always the heaviest sparticle in our setup, the following strong two body decay modes are the dominant gluino decay channels

$$\tilde{g} \to \tilde{t}_i t_i, \qquad \tilde{b}_i b_i \qquad i \in \{1,2\}.$$

There is no tree-level coupling between the squarks and the singlino in the NMSSM and thus the decays to neutralino states with a significant singlino component are suppressed. As the λ_S scenario contains an almost pure singlino LSP, direct decays of the squarks to the LSP very rarely occur. Even in the λ_L scenario, which can contain an LSP that is a Higgsino-singlino mix, the large singlino component significantly suppresses the direct decay to this state. This situation is different to the natural MSSM where stop decays into the LSP are common and consequently we expect longer and more complicated decay chains in the natural NMSSM. A by-product of such longer decay chains is that the individual particles produced are necessarily softer and E_T^{miss} can be expected to be reduced.

However in common with the natural MSSM, the sparticles will decay in final states with third generation SM particles which will give rise to a high b-jet multiplicity,

$$\tilde{t}_i \to \tilde{\chi}^0_{2/3} t, \qquad \tilde{\chi}^+_1 b,$$
$$\tilde{b}_i \to \tilde{\chi}^0_{2/3} b, \qquad \tilde{\chi}^-_1 t.$$

In addition, the large expected squark mass splittings in the λ_S scenario can lead to the following squark-to-squark decays with additional gauge bosons and Higgs scalars

$$\tilde{t}_2 \to \tilde{t}_1 X^0, \qquad \tilde{b}_i X^+,$$
$$\tilde{b}_2 \to \tilde{b}_1 X^0, \qquad \tilde{t}_1 X^-,$$

with $X^0 \in \{Z^0, h, H, H_3, A_1, A_2\}$ and $X^\pm \in \{H^\pm, W^\pm\}$. As the production rate of the heavy squark in such a case is largely suppressed compared to $\tilde{t}_1/\tilde{b}_1$, this decay is however not expected to contribute significantly to the observed event rates.

The biggest difference between the natural MSSM and the natural NMSSM is that we can now have a singlino LSP. This leads to additional decays of the (now next to LSP (NLSP)) Higgsinos $\chi^0_{2/3}$ such as

$$\tilde{\chi}^0_{2/3} \to \tilde{\chi}^0_1 X^0$$
$$\tilde{\chi}^\pm_1 \to \tilde{\chi}^0_1 X^\pm.$$

Generally, a light singlino is accompanied by relatively light singlet scalars. Depending on the mass difference between the NLSP and the LSP and the mass of the decay products X, differences between the MSSM and the NMSSM will arise, which may modify the decay patterns of the Higgsino in a MSSM scenario.

Of course, for each of the above listed decays there exists a mode with all involved particles charge conjugated. Obviously the listed decay modes are only possible subject to kinematic constraints and all decay modes mentioned above can have a related three (or four) body decay mode if one (or more) of the final state particles are virtual.

We have not listed the tediously large list of possible decays for the neutral scalars $\{h, H, H_3, A_1, A_2\}$: They generally involve Standard-Model-like Higgs decays, decays of heavy into light scalars and decays of heavy scalars into pairs of lighter squarks or electroweakinos. However, in most cases the heavy scalars H, H_3 and A_2 do not appear in the observed decay chains and thus their decay modes are of no relevance in the following. It is mostly the Standard-Model-like Higgs and the singlet-like scalars which are of importance and their decays are practically Standard Model like after having applied the experimental constraints as explained in upcoming Sec. III A.

III. MODEL TEST METHODOLOGY

As described at the end of Sec. II A, our model of interest can be described by 12 free parameters. To simplify the discussion, we assume a degeneracy[2] of the soft parameters in the third generation, i.e.

$$A_{\tilde{q}3} \equiv A_t = A_b, \tag{21}$$

$$M^2_{\tilde{q}3} \equiv m^2_{Q_3} = m^2_{U_3} = m^2_{D_3}. \tag{22}$$

This assumption always fixes the mass of the bottom squarks for given stop masses in a way as depicted in Fig. 1. In the following we explain how we fix the free parameters of our model:

$$\lambda, \quad \kappa, \quad A_\lambda, \quad A_\kappa, \quad \mu_{\text{eff}}, \quad \tan\beta, \quad A_{\tilde{q}3}, \quad M_{\tilde{q}3}, \quad M_3 \tag{23}$$

with respect to the hierarchies of the models we want to consider. We follow with a discussion on how we test the respective parameter combination.

A. Scan setup and definitions

Each of the data points that we are going to analyze is solely defined by the following set of information:

(1) The NMSSM scenario λ_S or λ_L,
(2) the mass $m_{\tilde{g}}$ of the gluino,
(3) the mass $m_{\tilde{t}_1}$ of the lightest stop,
(4) the Higgsino mass parameter μ_{eff} and
(5) the singlino mass parameter $m_{\tilde{S}} \equiv 2\kappa s$

This fixes the following parameters in Eq. (23):

$$\begin{aligned} \lambda &= 0.7(0.01) \quad \text{for } \lambda_L(\lambda_S), \\ \tan\beta &= 2(15) \quad \text{for } \lambda_L(\lambda_S), \\ \kappa &= \lambda/2 \cdot m_{\tilde{S}}/\mu_{\text{eff}} \quad \text{due to } \mu_{\text{eff}} = \lambda s. \end{aligned} \tag{24}$$

The remaining five parameters are found as follows: We require a natural, realistic particle content, that is we aim for a spectrum with as light as possible stops while having a Higgs boson at the correct mass. In addition we demand that the Higgs boson passes the most relevant theoretical and phenomenological constraints. Such a spectrum is found by using the public tool NMSSMTools [58–62]. This allows us to specify the above mentioned parameters at scale Q_t to get the corresponding physical particle masses, mixing matrices, branching ratios and test against a variety of observational tests (see below).

In order to find a parameter combination with a viable, natural spectrum, we perform the following chain of actions:
Loop over the heavy stop mass $m_{\tilde{t}_2}$ We are interested in stops that are as light as possible, i.e. we aim to find the lightest spectrum that passes the most important phenomenological constraints. For that purpose, with $m_{\tilde{t}_1}$ set above, we perform a loop over $m_{\tilde{t}_2}$: starting from $m_{\tilde{t}_1} + 25$ GeV and using a step size of 5 GeV, we steadily increase the heavy stop mass and try to find a valid parameter point according to the steps described next. As soon as a valid point is found, that one is taken for the further collider study.
Fix the strong sector M_3, $A_{\tilde{q}3}$, $M_{\tilde{q}3}$ The masses of the stops and the gluino are mostly determined by these three parameters. Given the target values $m_{\tilde{t}_1}$, $m_{\tilde{g}}$ and the looped value for $m_{\tilde{t}_2}$, we use NMSSMTools[3] to scan over M_3, $A_{\tilde{q}3}$ and $M_{\tilde{q}3}$ and find the combination that reproduces the desired masses[4] best. For this scan, the values of A_λ and A_κ are barely of relevance as they have only a minor impact on

[2]To be more precise, the degeneracy is assumed to hold at the scale $Q_{\text{SUSY}} = 5$ TeV with the exact choice being of minor relevance for the numerical results. Note that this is also the scale to which we put the decoupled SUSY particles.

[3]NMSSMTools has been modified to allow scanning over $A_{\tilde{q}3}$ and $M_{\tilde{q}3}$ which the public version does not allow.

[4]The mass calculation performed by NMSSMTools first uses 2-loop renormalization group equations to run the parameters from Q_{SUSY} down to $Q_{\tilde{t}} = M_{\tilde{q}3}$ and then evaluates the pole mass at $Q_{\tilde{t}}$ using next-to-leading order corrections in $\mathcal{O}(\alpha_s)$.

the third generation stop masses. Consequently they are therefore fixed to the central values of the "scalar sector scan" described below. Note that at this stage we use NMSSMTools solely to find the correct mapping of physical masses to parameters. No phenomenological constraints are applied at this stage.

Explore the scalar sector A_λ, A_κ Having the strong sector fixed we start a new grid scan over the scalar trilinear parameters A_λ, A_κ in order to find a phenomenologically allowed scalar sector. We test A_λ uniformly in the range 0 to $2(\mu_{\rm eff}/\sin 2\beta - m_{\tilde{S}})$, which is chosen such that the central value minimizes the Higgsino-singlino mixing in Eq. (9) and hence maximizes the SM-like Higgs boson mass [68]. A_κ is uniformly scanned in the range [−550 GeV, 450 GeV].

For each point, NMSSMTools tests

(i) the absence of tachyonic masses and charge or color breaking minima in the scalar potential,
(ii) that there is a SM-like Higgs boson in the mass window 121 to 129 GeV,[5]
(iii) consistency with all other implemented collider constraints (mostly Large electron positron collider limits on the Higgs sector, neutralinos and charginos)
(iv) consistency with all other implemented low energy observables. (e.g. $b \to s\gamma, B_s \to \mu^+\mu^-, \ldots$) apart from $(g-2)_\mu$ where our natural model will reproduce the SM expectation.

To consider more recent collider results from Large electron positron collider, Tevatron and the LHC that constrain the scalar sector, we further use HiggsBounds 4.1.2 [64] and HiggsSignals 1.2.0 [63] to perform final tests on the scalar sector of the considered parameter points. For that purpose we fix the mass uncertainty for all Higgs bosons to be 4 GeV. HiggsBounds is used with the LandH setup. A parameter combination is discarded if HiggsBounds returns "excluded." In HiggsSignals, the "both" setting is used that performs both a mass centered and a peak centered method using LATESTRESULTS. A point is discarded if it produces a p value smaller than 0.05.

Exit $m_{\tilde{t}_2}$ scan If at the end of this stage no allowed A_λ, A_κ combination is left, the $m_{\tilde{t}_2}$ loop starts with the next iteration. If however a parameter combination of M_3, $A_{\tilde{q}3}$, $M_{\tilde{q}3}$, A_λ and A_κ passes all the aforementioned constraints, this parameter point is used for collider phenomenology part described next.

For completeness it should be noted that the 5 parameters mentioned at the beginning of this section are closely related to the physical electroweakino masses. Firstly due to the decoupled wino, the mass of the chargino, $m_{\tilde{\chi}_1^\pm}$, is practically identical to the input parameter $\mu_{\rm eff}$ and we will therefore use both variables synonymously in the following. As depicted in Fig. 1, $\mu_{\rm eff}$ (or $m_{\tilde{\chi}_1^\pm}$) is also very close to the mass of the two neutral Higgsinos within λ_S. Likewise, the singlino mass parameter $m_{\tilde{S}}$ sets the mass of the lightest neutralino, $m_{\tilde{\chi}_1^0}$. Within λ_L however, large mixing in the neutralino sector will lead to deviations from these identities. In the following, instead of the input variable $m_{\tilde{S}}$ we will only show the physical mass of the lightest neutralino, $m_{\tilde{\chi}_1^0}$, which by construction is predominantly singlino like.

B. Collider phenomenology

As explained in Sec. II C, we assume that pair production of the light $\tilde{g}, \tilde{t}_i$ and $\tilde{b}_i$ dominates the expected signal. Production cross sections for these particles are calculated using NLLFast 2.1 [70–76] using CTEQ6.6NLO parton distribution function [77]. Uncertainties due to scale variations, parton density functions and α_s are provided and we take the quadratic sum of these to set the total theory error $\Delta\sigma$. For each production mode, 50 000 signal events are generated using Herwig++ 2.7.0 [78,79] with the NMSSM model setting. For practical reasons, decay tables of all relevant particles are calculated within Herwig++, which contains all tree-level 2- and 3-body decays and effective implementations of the loop-induced decays $h_i \to \gamma\gamma, gg$.

To test the model against a variety of LHC results, we use CheckMATE [56,57]: This tool applies an ATLAS tuned version of the Delphes 3 [80] detector simulation which uses FastJet with the anti-k_T jet algorithm [81–83]. Reconstructed events are tested against various ATLAS analyses and the derived number of signal events is tested against observation and the Standard Model expectation. The compatibility of signal and observation is tested by comparing the predicted signal $S \pm \Delta S$ to the model independent 95% C.L. limit $S95$, determined by using the $\rm CL_S$ method [84]. Here, ΔS considers both the Monte Carlo error on our statistics as well as the theory error on the total cross sections. CheckMATE considers a large list of ATLAS analyses, however due to the signatures described in Sec. II C it is expected that only a subset of these will be sensitive to the characteristics of our model. We list these analyses in Table I. They all require a significant amount of missing transverse momentum due to the expected undetected LSP in the final state and have signal regions that check for b jets. They mainly differ by the final state jet multiplicities and the total amount and relative charge of final state isolated leptons (i.e. electrons and muons). The analyses also differ in the kinematics of the respective signal regions that are designed and tuned for particular final states. As we expect different final state signatures in our model, it is highly favorable to check all

[5]The window for m_h is motivated by theory uncertainties and the fact that the decoupled sector, most importantly the electroweakinos, can influence the Higgs mass by higher order corrections if they are of order $\mathcal{O}$(few TeV), see e.g. [69]. The exact details of the heavy electroweakino sector would not affect our collider analysis at all and thus are incorporated by a looser constraining on the light Higgs boson mass.

TABLE I. Summary of the expected most sensitive analyses within CheckMATE to the considered natural model, listed in alphabetical order. All analyses require a significant amount of missing transverse momentum in the final state and have at least one signal region which requires b-tagged jets. All other ATLAS analyses implemented in CheckMATE are tested in parallel, but are always found to be less sensitive than those listed.

Reference	CheckMATE identifier	Sensitive to which decay scenario(s)
[49]	atlas_conf_2013_024	stop/sbottom decay chains leading to purely hadronic final states
[52]	atlas_conf_2013_061	$\tilde{g}\tilde{g} \to t\bar{t}\tilde{t}\tilde{t}^*, b\bar{b}\tilde{b}\tilde{b}^*$ and/or decays involving $h \to b\bar{b}$.
[85]	atlas_conf_2013_062	stop/sbottom decay chains with 1 isolated lepton from W/Z
[86]	atlas_1308_2631	$\tilde{t} \to b\tilde{\chi}^{\pm}, t\tilde{\chi}^0$ with a purely hadronic final state
[87]	atlas_1403_4853	$\tilde{t} \to b\tilde{\chi}^{\pm}, t\tilde{\chi}^0$ with an opposite sign isolated lepton pair in the final state
[88]	atlas_1404_2500	$\tilde{g}\tilde{g}$ with decays into stop/sbottom producing 2 same sign or 3 isolated leptons
[48]	atlas_1407_0583	stop/sbottom decay chains with 1 isolated lepton from W/Z

these possibilities in parallel and filter out the most sensitive one for each case. Fortunately, CheckMATE allows for an easy comparison of that kind.

IV. RESULTS

In the following we show exclusion lines in the parameter space of the model explained above. Since we still have $m_{\tilde{g}}, m_{\tilde{t}_1}, m_{\tilde{\chi}_1^{\pm}}$ and $m_{\tilde{\chi}_1^0}$ as continuous degrees of freedom, we choose to present results for specific chosen benchmark scenarios.

As one of our considered decay chains in Sec. II C starts with the production of gluinos and ends with the decay into the singlino LSP, we first choose to show exclusion lines in the plane spanned by the masses of these two particles. We do so for various choices of $m_{\tilde{t}_1}, m_{\tilde{\chi}_1^{\pm}}$ and always compare the results for λ_L and λ_S. As it will turn out, light gluinos mostly lead to severely constrained models. Thus we will follow with a scenario in which the gluino is decoupled from the spectrum as well. We then show exclusion lines in the $m_{\tilde{t}_1} - m_{\tilde{\chi}_1^0}$ plane for different chargino masses, again putting the results for λ_L and λ_S side by side. For the specific case of a light LSP, we also present results in the $m_{\tilde{t}_1} - m_{\tilde{\chi}_1^{\pm}}$ plane to illustrate the dependence on the chargino mass for both λ scenarios.

To keep the discussion compact, we only show 95% exclusion lines in different parameter planes within this section. An exhaustive list of plots showing distributions of masses, cross sections and branching ratios can be found in Figs. 13–23 within the Appendices.

A. Gluino-LSP plane

In Figs. 2–6 we show the 95% exclusion region in the gluino-LSP mass plane, using fixed stop masses in the range $m_{\tilde{t}_1} = 400$ to 800 GeV. For each case, the λ_L and λ_S scenarios are compared in the left and right panel, respectively. Within each panel we compare the exclusion regions for different chargino mass values that obey $m_{\tilde{\chi}_1^{\pm}} \leq m_{\tilde{t}_1}$. We note that if the chargino is heavier than the stop it does not contribute to the dominant decay chains and thus the limits are practically the same as the case $m_{\tilde{\chi}_1^{\pm}} = m_{\tilde{t}_1}$. Since the chargino must not be lighter than the LSP, each exclusion line has an individual upper limit on the $m_{\chi_1^0}$ axis, drawn by dashed horizontal lines.[6] Chargino mass values that are listed in the legend but do not appear in the plot should be interpreted as being entirely excluded across the whole mass plane.

We display results for gluino masses, $m_{\tilde{g}} \geq 900$ GeV, since below this mass, the exclusion relies on at least one hard jet that originates from initial state radiation. Unfortunately Herwig++ is not able to include such radiation at the matrix element level and is therefore unable to provide reliable results in this region of parameter space. However, we note that we expect the results to be very similar to the MSSM here because the decay products of the gluino become soft as the mass splitting to the LSP becomes small. Since the particles become harder to reconstruct, differences in exclusions due to different decay topologies will become more difficult to distinguish. We note that in the limit that the gluino is degenerate with the LSP, the bound is approximately $m_{\tilde{g}} \geq 500$ GeV [89,90]

Generally, the exclusion lines split the parameter space into two regions of interest and we discuss these regions separately:

1. Light gluinos

For $m_{\tilde{g}} \lesssim 1100$ GeV, Figs. 2–6 show that the limits are mostly independent of the chargino mass and apparently primarily driven by the gluino decay products in the decays $\tilde{g} \to \tilde{b}b, \tilde{t}t$.

As the bounds in that region do not seem to vary significantly as we change the mass of the electroweakinos

[6]For given $m_{\tilde{\chi}_1^{\pm}} \approx \mu_{\text{eff}}$, this theoretical upper limit should appear for $m_{\tilde{\chi}_1^{\pm}} = m_{\tilde{\chi}_1^0}$. However, since μ_{eff} also sets the scale of the neutral Higgsinos in our setup, mixing in the neutralino sector does not allow for points which fulfill the equality. Therefore the dashed horizontal lines appear slightly below the $m_{\tilde{\chi}_1^{\pm}} = m_{\tilde{\chi}_1^0}$ line, namely at the heaviest singlino-like $\tilde{\chi}_1^0$ that can be achieved for given μ_{eff}.

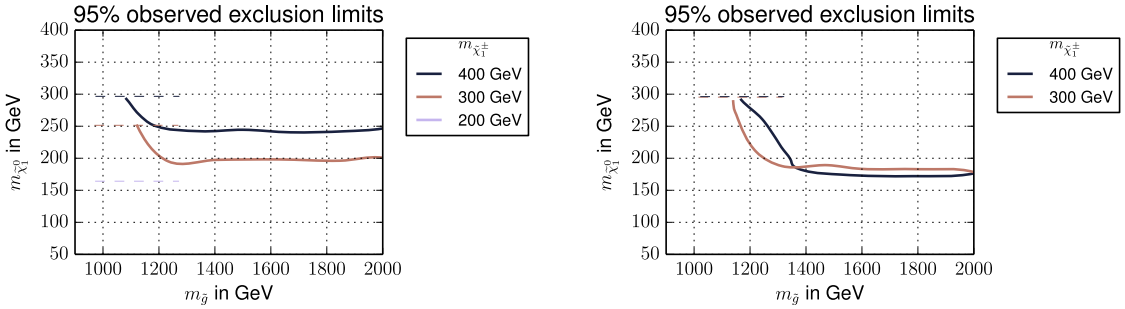

FIG. 2. Observed 95% C.L. exclusion limits for $m_{\tilde{t}_1} = 400$ GeV. Left: λ_L. Right: λ_S.

(and only barely if we change the mass of the lightest stop), we conclude that the details of the decay chain of the third generation scalars into the LSP is almost irrelevant when setting limits on the model. The only exception is if very small mass splittings occur in the decay chain, for example between the gluino and the stop or the stop and the Higgsinos. We can see the effect in the left parts of Fig. 6 and also can be observed for all scenarios with $m_{\tilde{\chi}_1^\pm} \lesssim m_{\tilde{t}_1}$ in Figs. 4–6.

When we compare the λ_S and λ_L limits we also see that the limits are stable between the two scenarios once gluino production is dominant. Consequently, we again conclude that the precise decay modes of the $\tilde{t}(\tilde{b})$ and the various $\tilde{\chi}_1^0, \tilde{\chi}_1^\pm$ do not effect the LHC phenomenology in this region of parameter space.

The above conclusions may be different to the thoughts we had before commencing this study. In fact we may have guessed that the additional decay step present due to the singlino would have made the model more difficult to see at the LHC. The reason is that the extra decay can reduce the individual final state particle energies and also the total missing energy (e.g. [91]). We believe the reason that this does not occur here is the number of studies and therefore signal regions contained within the CheckMATE program. For example, in Fig. 7, we can compare the respective most constraining signal regions in the gluino-dominated region for a specific benchmark scenario. We see that the signal regions used to constrain the models are different between the two scenarios. In particular the λ_S scenario which generically contains longer decays is better constrained by signal regions that have a larger final state particle multiplicity. For instance, in the gluino-dominated region, the ATLAS search with at least 3 b jets [52] (atlas_conf_2013_061) is the most powerful but while the λ_L scenario is best constrained with the 4-jet signal region, the 6-jet + 1-lepton region dominates for λ_S. In addition, the multi b-jet ATLAS search demands moderate missing

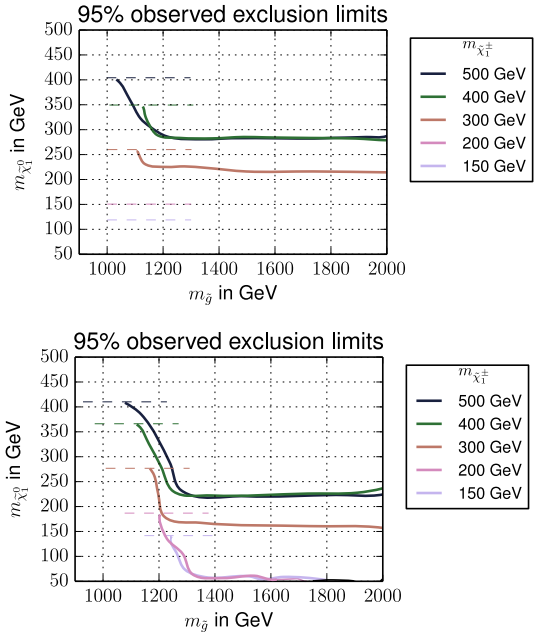

FIG. 3. Observed 95% C.L. exclusion limits for $m_{\tilde{t}_1} = 500$ GeV. Top: λ_L. Bottom: λ_S.

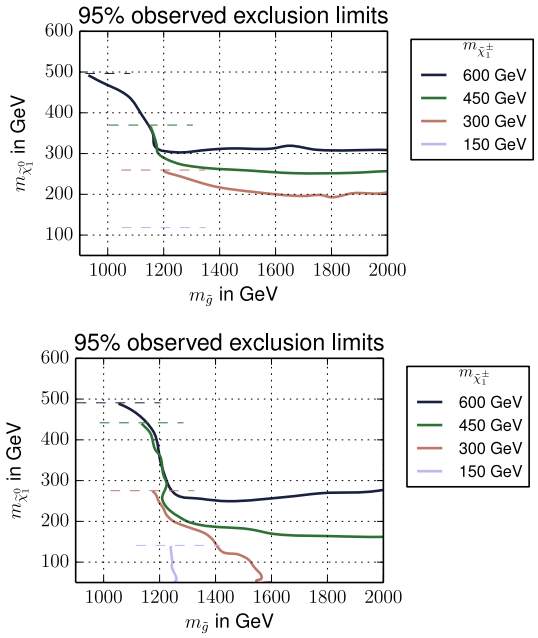

FIG. 4. Observed 95% C.L. exclusion limits for $m_{\tilde{t}_1} = 600$ GeV. Top: λ_L. Bottom: λ_S.

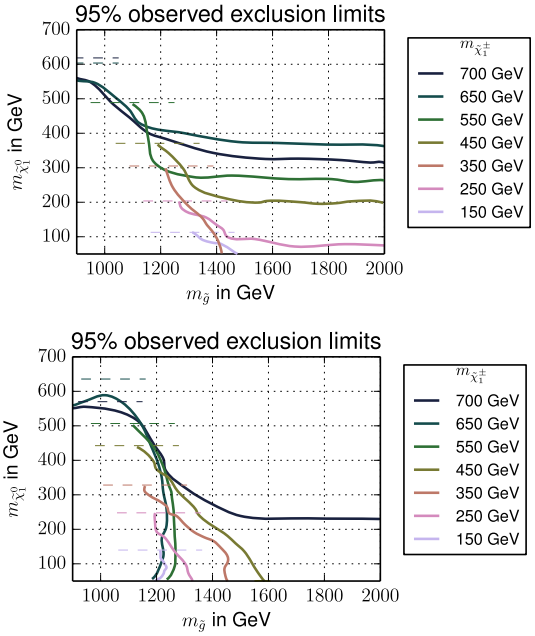

FIG. 5. Observed 95% C.L. exclusion limits for $m_{\tilde{t}_1} = 700\,\text{GeV}$. Top: λ_L. Bottom: λ_S.

transverse momentum and hence the reduction of the total missing energy in the NMSSM does not significantly change the efficiency in the signal regions. The demands of the signal region therefore translates into the necessity of a sufficiently large gluino production cross section and a sizeable mass splitting of gluinos and squarks as well as squarks and electroweakinos. It is thus expected that limits should not depend significantly on the λ scenario and only

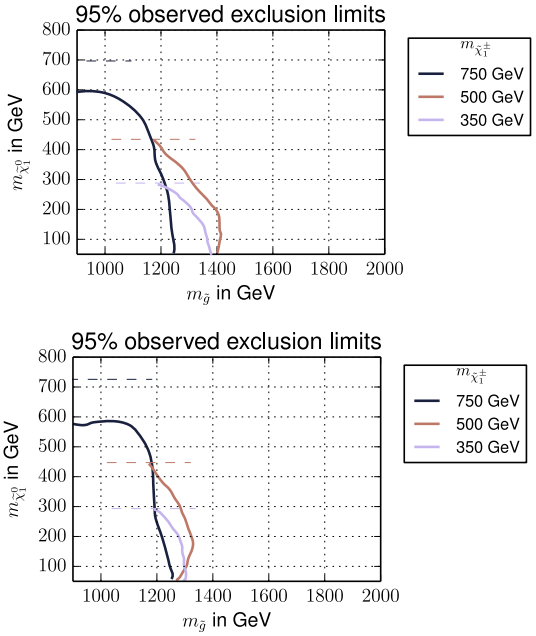

FIG. 6. Observed 95% C.L. exclusion limits for $m_{\tilde{t}_1} = 800\,\text{GeV}$. Top: λ_L. Bottom: λ_S.

on the masses if they are close to threshold, as can be seen in our results.

2. Heavy gluinos

For gluinos with mass above the production threshold of about 1.2 TeV, the exclusion sensitivity will be dominantly driven by the production of the third generation sparticles $\tilde{t}_{1/2}, \tilde{b}_{1/2}$ if they are sufficiently light. To illustrate this, we show the total production cross section for gluinos in Fig. 14 of Appendix B and third generation squark production for fixed $m_{\tilde{t}_1}$ in Fig. 15. Comparing the cross section values in regions with $m_{\tilde{g}} > 1.2$ TeV, $m_{\tilde{t}_1} < 800$ GeV, one expects far more $\tilde{t}_1$ than gluinos to be produced. Depending on the λ scenario large numbers of events with sbottoms and heavier stops are expected in addition. Therefore, beyond the gluino threshold we observe a gluino-independent upper limit on the mass of the lightest neutralino.

However, contrarily to the gluino-dominated region, one now finds significant dependencies of the limits on the chargino mass parameter and the λ scenario in Figs. 2–6. In general, we observe that for a fixed mass of the lightest stop, limits on the LSP mass become weaker the lighter we chose the intermediate chargino. Also, throughout all cases we find consistently better limits in the λ_L scenario than for λ_S.

To understand these differences, we first have to shed light on the analyses and signal regions which define our exclusion limits in this part of parameter space. In Fig. 7, we take the specific example of a light stop mass of 500 GeV and show the most sensitive signal regions for chargino masses of 400 and 300 GeV, comparing λ_L on the left to λ_S on the right. One finds two main classes of final states to be of importance here:

(1) Signal regions from atlas_conf_2013_024 and "tN-type" regions in atlas_1407_0583 focus on final states that originate from direct $\tilde{t} \to t\tilde{\chi}_1^0$ decays. That is, they require missing transverse momentum, b jets and final state objects whose invariant mass lie close to the top-quark mass.

(2) "bC-type" regions in atlas_1407_0583 have been designed to tag events of type $\tilde{t} \to b\tilde{\chi}^\pm, \tilde{\chi}^\pm \to W^\pm\tilde{\chi}_1^0$ by using kinematic variables that are sensitive to intermediate decay steps.

In the following, we will refer to these as tN-like and bC-like analyses and signal regions, respectively.

In our model setup, the choice of the Higgs mass parameter μ (which sets the $m_{\tilde{\chi}_1^\pm}$ and $m_{\tilde{\chi}_{2,3}^0}$) is crucial to determine how many events are expected to be counted for the above most sensitive signal regions. Its value sets the kinematically open channels from the full list in Sec. II C, fixes the branching ratios and determines the energy distribution among the final state particles.

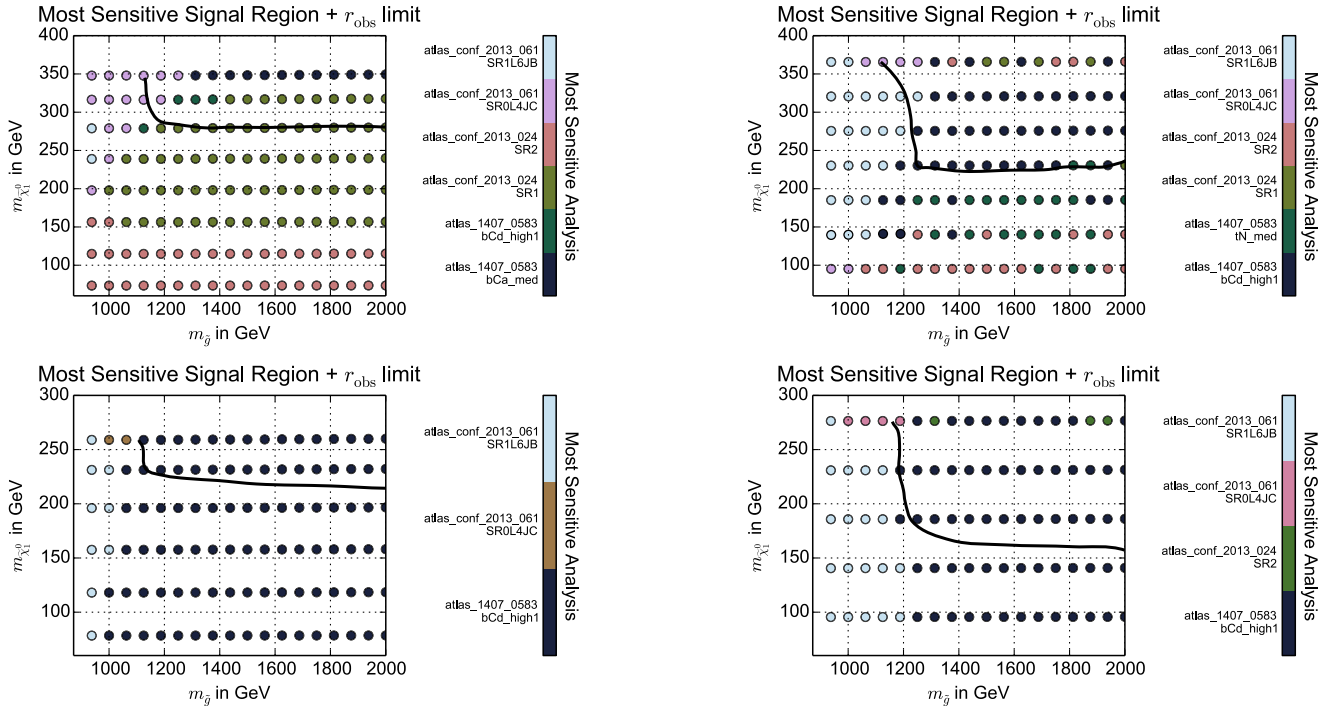

FIG. 7. Most sensitive signal region for each individual point in the gluino-LSP scan, using $m_{\tilde{t}_1} = 500$ GeV, $m_{\tilde{\chi}_1^\pm} = 400$ GeV (top) and 300 GeV (bottom). Left: λ_L. Right: λ_S.

For $m_{\tilde{\chi}_1^\pm} \geq m_{\tilde{\chi}_1^0}$, the branching ratio for $\tilde{t}_1 \to t\tilde{\chi}_1^0$ is almost 100%—regardless of λ—and thus the upper LSP mass limits in both scenarios are determined by results from tN-like signal regions. If the $\tilde{t}_1$ was the only squark kinematically available, the limits of λ_L and λ_S would be expected to coincide. Comparison of the corresponding $m_{\tilde{t}_1} = m_{\tilde{\chi}_1^\pm}$ lines in Figs. 2–6 however shows that λ_L yields stronger limits, with the difference being larger for lighter $m_{\tilde{t}_1}$. The reason here is that λ_L can allow for additional lighter 3rd generation squarks while still being able to get the right SM Higgs mass, as in Eq. (19). These lighter squarks have a larger production cross section and thus contribute more to the observable events, e.g. via decays $\tilde{b}_1 \to t\tilde{\chi}_1^\pm$ which can also pass the signal region cuts. If a light $\tilde{t}_1$ is present in a λ_S scenario however, the additional 3rd generation squarks are required to be much heavier.

For lighter chargino masses, the decay $\tilde{t}_1 \to b\tilde{\chi}_1^\pm$ opens kinematically. Within the λ_S scenario we have an almost purely singlino LSP which causes the branching ratio for $t\tilde{\chi}_1^0$ final states to become almost immediately disfavored below the chargino threshold. Thus in this scenario almost all stops have to decay via intermediate electroweakinos. Interestingly, tN-like analyses are still most significant to set the limit if the charginos are not too light (see Fig. 7 top right). The reason is that events with intermediate charginos can lead to $bW^+\tilde{\chi}_1^0$ final states misidentified as top quarks within tN-like signal region selections if the neutralino is light enough (the top mass window is very large in this analysis, as wide as $130 < m_t < 250$ GeV). In addition one expects a significant contribution of sbottoms decaying into $t\tilde{\chi}_1^\pm$ final states which also look tN like.

For even lighter charginos, the limit is however only set by bC-like analyses (see Fig. 7). Decreasing the chargino mass further leads to softer decay products in the decay $\tilde{\chi}_1^\pm \to \tilde{\chi}_1^0 X^\pm$, which weakens the resulting upper limits on the $\tilde{\chi}_1^0$ mass. Finally, decays into $t\tilde{\chi}_{2/3}^0$ can reduce the branching ratio into the above mentioned decays once the chargino becomes light enough (see Fig. 16).

It should also be mentioned that the branching ratios of the stop into neutral and charged Higgsinos are fixed by the stop mixing matrix and $\tan\beta$ [92,93]. This results in a significant number of events displaying an "asymmetric" topology in which each of the initially produced sparticles decays differently. However, the signal regions within the analyses that we use are mainly designed for symmetric decay scenarios, which leads to a reduction of the overall sensitivity.

Most of the explanations in the above discussion apply similarly to the λ_L scenario. However, a distinctive feature is the strong mixing in the neutralino sector which allows for the LSP to have a large Higgsino component and thus $t\tilde{\chi}_1^0$ decays still having a large branching fraction below the chargino threshold. For example one finds that for $m_{\tilde{t}_1} - m_{\tilde{\chi}_1^\pm} \lesssim 150$ GeV direct stop-to-top decays still happen with more than 20% probability (see Fig. 16). We therefore expect, and observe, that also within λ_L the tN signal regions set the limit for charginos within that mass region (see Fig. 7, top left).

For lighter charginos, the limits become weaker due to the decreasing branching ratio of the "golden channel" $\tilde{t}_1 \to t\tilde{\chi}_1^0$ and eventually the bC signal regions dominate and sets the limits thereafter (see Fig. 7, bottom left). The overall stronger exclusions within the λ_L scenario can therefore be attributed to two different reasons. Firstly, the other 3rd generation squarks will again be lighter in the λ_L scenario due to the additional singlet contributions to the Higgs mass. Secondly, the increased branching ratio of $\tilde{t}_1 \to t\tilde{\chi}_1^0$ which the LHC analyses are particularly sensitive to also helps.

Interestingly, in both λ scenarios, μ_{eff} lighter than $m_{\tilde{t}_1} - m_t$ opens decay channels of the type $\tilde{t}_1 \to t\tilde{\chi}_{2/3}^0$. These could lead to NMSSM-specific final states as discussed in Sec. II C. However, we do not observe any improvement on the LSP limits in these cases. Quite the contrary, the reduction of the branching ratio into $b\tilde{\chi}_1^\pm$ final states resulting from the new decay channel and asymmetric final states mentioned above weakens the limits even more as can be observed when comparing the limits in Figs. 2–6 above or below this threshold. We investigate the impact of this more closely in the upcoming section.

B. Stop-electroweakino plane

As shown in the last set of results, below the gluino production threshold, the LHC limits only have a small dependence on the details of the natural spectrum. However, as we decouple the gluino, the masses and couplings of the electroweakino sector become more important. For that reason we also show results in the $m_{\tilde{t}_1}$-$m_{\tilde{\chi}_1^0}$ plane for a decoupled gluino of mass 2 TeV in Figs. 8–11. With 1 degree of freedom less, we are now able to show one exclusion limit per plot for specific values of $m_{\tilde{\chi}^\pm}$, again comparing λ_L (left) to λ_S (right). The parameter space that we investigate does not include the region where $m_{\tilde{t}_1}$ becomes close to $m_{\tilde{\chi}_1^0}$. This is shown by the diagonal dashed line within each plot which shows the kinematic range for which $m_{\tilde{t}_1} < m_b + m_W + m_{\tilde{\chi}_1^0}$ and only 4-body final states or flavor changing neutral current decays such as $\tilde{t}_1 \to c\tilde{\chi}_1^0$ are possible. Given the small mass difference, initial state radiation searches provide the most constraining limits in this region [94,95]. These searches are relatively insensitive to the details of the decay chain in question and thus we expect the results to be very similar to those of the MSSM.

Similarly to the gluino-LSP scan, the upper limit on the LSP mass is set by requiring $m_{\tilde{\chi}_1^0} < m_{\tilde{\chi}^\pm}$. For the λ_L case, mixing in the neutralino sector leads to a maximum achievable value of $m_{\tilde{\chi}_1^0}$ which lies somewhat below $m_{\tilde{\chi}^\pm}$. In the λ_S scenario, realistic parameter points are not possible with $m_{\tilde{t}_1} \lesssim 400$ GeV if $m_{\tilde{\chi}^\pm} \approx \mu_{\text{eff}}$ is small. The reason is that for small μ_{eff} and small $m_{\tilde{t}_1}$, both the tree-level and radiative contributions to the Higgs boson mass are not large enough to correctly reproduce the LHC measurement [see e.g. Eq. (19)].

In all plots we again show, for each individual considered data point, the most sensitive analysis that has been used to calculate the confidence level of that particular point. However, we do not show the numerous individual signal regions (as we did for Fig. 7) to keep the amount of different values to a reasonable level.

We again observe that the choice of analysis responsible for the limit setting is strongly correlated with the branching ratio of the lightest stop and from Fig. 16 we expect four main regions of interest. These are respectively, direct decays of the stop into the LSP and an (a) on- or (b) off-shell top, (c) intermediate decays via charginos or (d) via neutral Higgsinos. The thresholds for these regions often coincide with similar threshold for sbottom decays, as can be seen in Fig. 18. As an example the $\tilde{b}_1 \to t\tilde{\chi}^\pm$ and the $\tilde{t}_1 \to t\tilde{\chi}_{2/3}^0$ lie very close in the λ_L scenario.

Using the branching-ratio information, we can closely follow the explanations from the last section to understand the limits in Figs. 8–11. For stops lighter than the given chargino, only direct decays $\tilde{t}_1 \to t^{(*)}\tilde{\chi}_1^0$ are kinematically allowed. tN-like analyses are therefore the most sensitive and lead to similar limits for λ_L and λ_S, with the former being slightly stronger than the latter due to the lighter sbottoms in this model. In λ_S, a strip for $m_{\tilde{t}_1} - m_{\tilde{\chi}_1^0} < m_t$

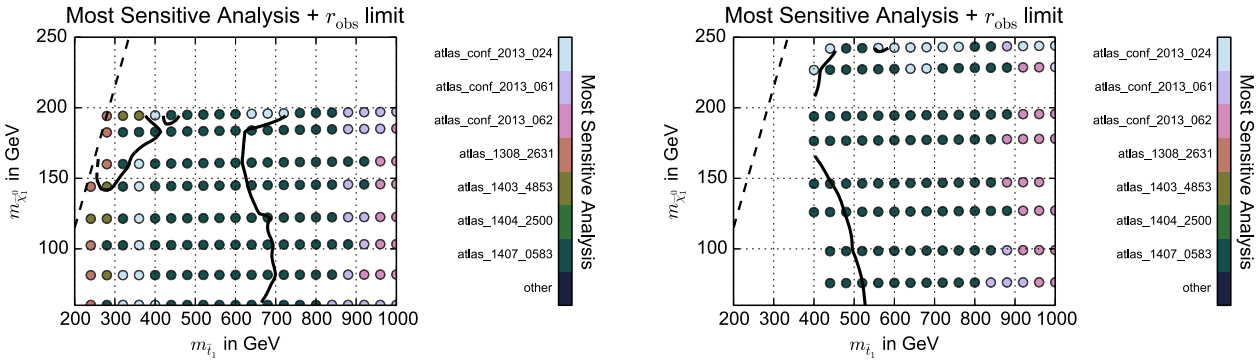

FIG. 8. Observed 95% C.L. exclusion limit and most sensitive analysis per point for $m_{\tilde{\chi}_1^\pm} = 250$ GeV. Left: λ_L. Right: λ_S.

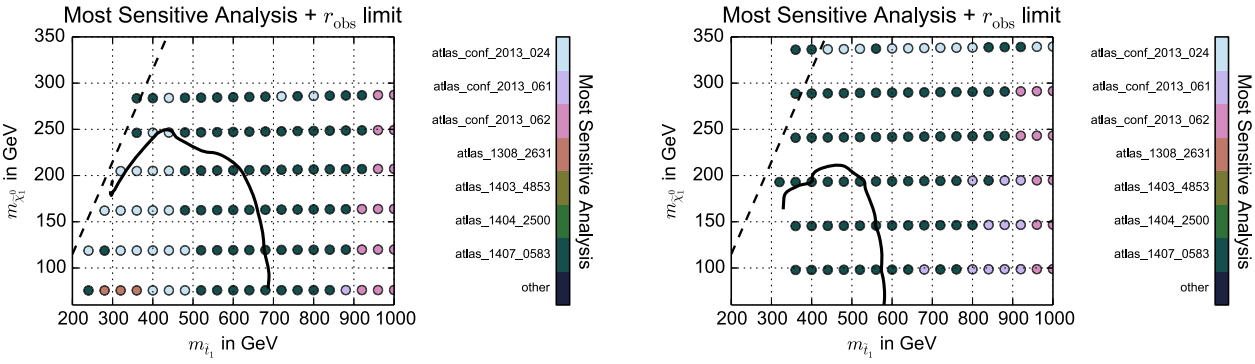

FIG. 9. Observed 95% C.L. exclusion limit and most sensitive analysis per point for $m_{\tilde{\chi}_1^\pm} = 350$ GeV. Left: λ_L. Right: λ_S.

cannot be excluded as the final state with an off-shell top is not observed by tN-like analyses and hard to distinguish from the SM background. Within λ_L, this region can still be explored since it is possible that the spectrum also contains a light $\tilde{b}_1$. This can be excluded via $\tilde{b} \to t\tilde{\chi}^\pm$ specific selections in `atlas_1404_2500` (see e.g. Figs. 10,11).

For kinematically allowed chargino decays, a transition from tN into bC signal regions can be observed for increasing $m_{\tilde{t}_1}$, that is for larger stop-chargino splitting. As in the previous setup, λ_L profits from the Higgsino fraction of the LSP and the generally lighter 3rd generation squarks. The highest sensitivities are reached via tN final states in atlas_conf_2013_024. The highest sensitivity to the LSP mass can be reached when these final states set the limit, which can reach up to $m_{\tilde{\chi}_1^0}^{\rm max} \approx 325$ GeV. In λ_S, `bC` signal regions dominate the limit earlier, which require lighter neutralinos to observe the intermediate chargino decay step. The experimental reach to the LSP mass is therefore smaller in these scenarios and of order 250 GeV.

As we further increase the stop masses, a maximum value of $m_{\tilde{t}_1}$ is reached. This stop sensitivity limit seems to depend on the chosen chargino mass and the considered λ scenario and is rather independent of the LSP mass as long as it is light enough, that is for $m_{\tilde{\chi}_1^0} \lesssim 150$ GeV.

To better understand the parameter dependence, we chose to show results in the $m_{\tilde{t}_1}$-$m_{\tilde{\chi}_1^\pm}$ plane for a fixed, light LSP mass of 100 GeV in Fig. 12. We show the previously discussed thresholds for $\tilde{t}_1 \to b\tilde{\chi}^\pm$ and $\tilde{t}_1 \to t\tilde{\chi}_{2/3}^0$ and it can be seen that they can have an important impact on the sensitivity of the experimental analyses to the stop mass. Within λ_L, the lower limit on $m_{\tilde{t}_1}$ is almost constant at ≈700 GeV for charginos above the $t\tilde{\chi}_{2/3}^0$ threshold. This corresponds to similar limits from simplified $\tilde{t} \to t\tilde{\chi}_1^0$ topologies as in [48,49]. The limit gets slightly weaker if the chargino threshold is passed, dropping by at most 50 GeV as soon as bC signal regions dominate the limit. In Figs. 17,19 and 21 we show the branching-ratio distributions in the same plane and the same LSP mass as the results in Fig. 12. One observes that the mass values in our spectrum are such that the above behavior coincides with the threshold for $\tilde{b} \to t\tilde{\chi}^\pm$, which also explains why the bC-like signal regions become important within this region of parameter space.

As long as the Higgsinos do not appear in the squark decay chains, λ_S returns similar limits as the λ_L scenario, for the same reasons discussed in the previous section. However, within this model one observes a sizeable weakening of the limits as soon as the intermediate chargino and NLSP Higgsino decays open kinematically. Interestingly, the latter has a particularly negative impact on the result, as the experimental analyses are only weakly sensitive to parameter regions in λ_S where $\tilde{t}_1 \to t\tilde{\chi}_{2/3}^0$ is

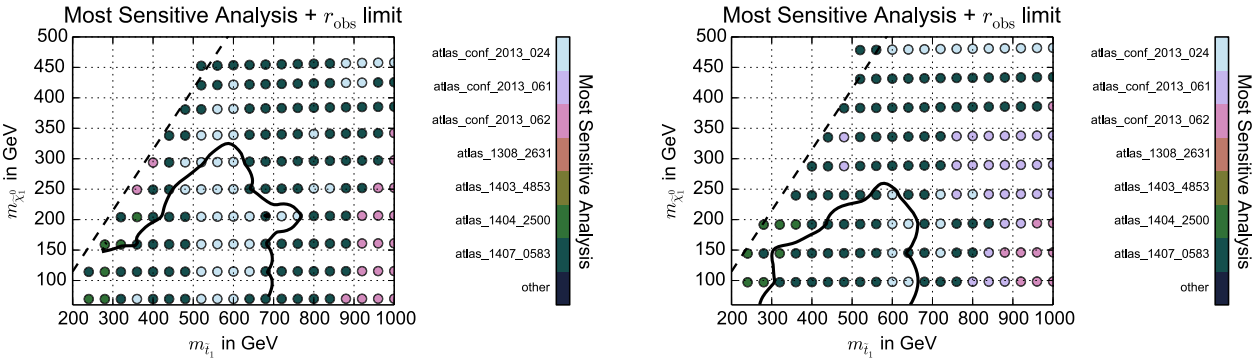

FIG. 10. Observed 95% C.L. exclusion limit and most sensitive analysis per point for $m_{\tilde{\chi}_1^\pm} = 500$ GeV. Left: λ_L. Right: λ_S.

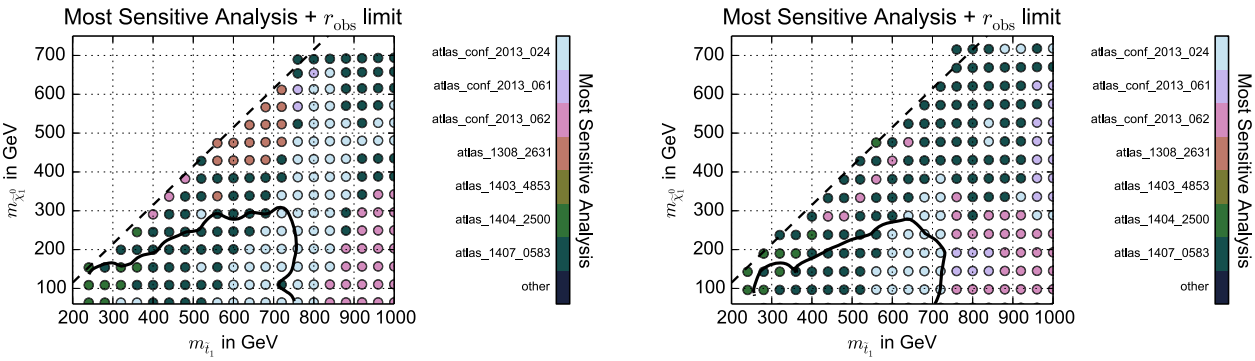

FIG. 11. Observed 95% C.L. exclusion limit and most sensitive analysis per point for $m_{\tilde{\chi}_1^\pm} = 750$ GeV. Left: λ_L. Right: λ_S.

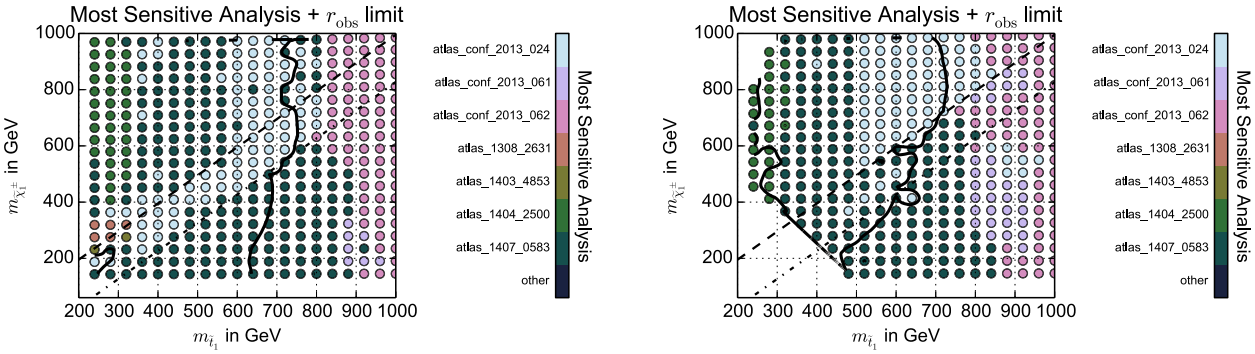

FIG. 12. Observed 95% C.L. exclusion limit and most sensitive analysis per point for $m_{\chi_1^0} = 100$ GeV. Diagonal dashed (dashed-dotted) lines show shows the threshold for $\tilde{t}_1 \to b\tilde{\chi}_1^\pm$ ($\tilde{t}_1 \to t\tilde{\chi}_{2/3}^0$). Left: λ_L. Right: λ_S.

kinematically allowed. As discussed in Sec. II C, it is this decay chain which yields NMSSM-specific features in the final state topology: the decay of the Higgsino NLSPs into the singlino LSP should create a sizeable excess of $h/H/A_1 \to \bar{b}b$ final states. It seems, however, that none of the many distinct final states within the numerous analyses that CheckMATE contains is sufficiently sensitive to this topology. Thus, the existing bC-like limits are weakened due to reduced branching ratios after passing the NLSP Higgsino threshold. The weakened limits can be clearly seen in Fig. 12 where for light $\chi_1^\pm$ (and $\chi_{2,3}^0$) states, the limit on the stop mass drops from $m_{\tilde{t}} \geq 650$ GeV when the longer decay chains are not important to $m_{\tilde{t}} \geq 450$ GeV when they dominate.

We therefore conclude that not only can many limits on natural NMSSM scenarios be derived from very similar topologies in natural MSSM studies, but we also find that regions of parameter space which produce NMSSM-exclusive final state features are not sufficiently covered by existing studies. Therefore, only weak limits on the NMSSM can be set within this region of parameter space which suffer under branching-ratio penalties.

V. CONCLUSION

In this study we explore the natural NMSSM to determine how the additional singlino can effect the LHC searches compared to the more studied MSSM case. To do this we explored a number of different scenarios, mostly notably examining the difference between a small-λ case, where the LSP is dominantly a singlino and the large-λ case, where the LSP can contain a substantial Higgsino component. We also study in detail the differences that occur when the gluino is light enough that it dominates the SUSY production cross sections and what happens when the gluino is pushed to a mass where LHC production is no longer copious.

We find that, when constructing a realistic phenomenological model, the NMSSM-specific decay chains via intermediate heavy neutralinos often create an MSSM-like topology, $\tilde{q}_3 \to q_3\tilde{\chi}_1^0$ which can be preceded by $\tilde{g} \to \tilde{q}_3 q_3$ if the gluino is light. If the branching ratio to these decay chains are large, the limits very closely follow those often studied as simplified models in the MSSM. However, the branching ratio depends on the size of the NMSSM coupling λ. If it is large, all neutralinos have a sizeable Higgsino fraction and direct decays into the lightest neutralino are significant. However, in case of small λ, the coupling of the squarks to the LSP is made small since it has a large singlino content. Therefore decays via intermediate charged and neutral Higgsinos are preferred if kinematically allowed which lengthens the decay chains via $\tilde{t}_1 \to b\tilde{\chi}_1^\pm$ or $\tilde{t}_1 \to t\tilde{\chi}_{2/3}^0$. The heavier

chargino or neutralino states then go on to produce different combinations of gauge and Higgs bosons in their decays. In addition, since different decay modes may be competing with similar branching ratios, asymmetric decay chains can often occur.

These longer decay chains can lead to weaker LHC bounds for two particular reasons. First of all, the ATLAS searches have more focussed on the MSSM specific signatures and consequently not been designed with these final states in mind. Secondly, the longer decay chains lead to a higher final state particle multiplicity but with each individual particle carrying smaller p_T. In addition the same effect reduces the final state E_T^{miss} as observed in other studies with more complicated decay topologies e.g. [91]. On the other hand, additional final states, namely jets and leptons, can improve the sensitivity even though the invisible transverse momentum is reduced. Therefore an important conclusion of this study is that it is not obvious if the efficiency is smaller or larger in a particular NMSSM scenario simply by looking at the spectrum and decays. Instead it is crucial to test the model against a large number of searches covering various final state topologies. However, in our study we have found the general behavior that the regions of the natural NMSSM that are particularly weakened with respect to the MSSM are those with small λ coupling and light Higgsino states.

Within this study we do test a large variety of different analyses but still only use one signal region to define the overall limit. In the models with extended and asymmetric decay chains (where we observe a weakening of the LHC limit), we expect the signal to populate a more varied number of signal regions than if the model predicted a single dominating decay chain. Therefore it may be expected that a combination of the sensitivities across all analyses can significantly enhance the limits but this is beyond the scope of this study.

ACKNOWLEDGMENTS

J. T. would like to thank Professor Herbi Dreiner and the Bethe Centre for Theoretical Physics at Bonn University for hospitality and support while part of this work was completed. The work of J. S. K. has been partially supported by the MICINN, Spain, under Contract No. FPA2013-44773-P, Consolider-Ingenio CPAN CSD2007-00042 and the Spanish MINECO Centro de excelencia Severo Ochoa Program under Grant No. SEV-2012-0249.

APPENDIX A: MASS DISTRIBUTIONS

An exhaustive list of plots showing distributions of masses.

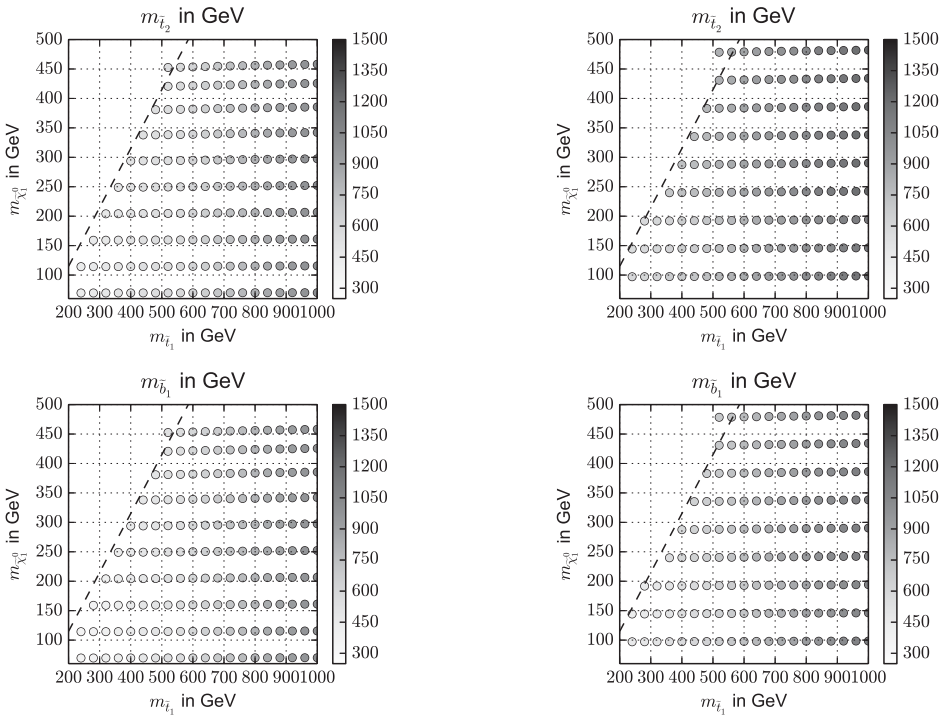

FIG. 13. Mass of the heavier stop and the lighter sbottom (which is very degenerate with the heavier sbottom) for a decoupled gluino and $m_{\tilde{\chi}_1^\pm} = 500$ GeV. Left: λ_L. Right: λ_S

APPENDIX B: CROSS SECTION DISTRIBUTIONS

An exhaustive list of plots showing distributions of cross sections.

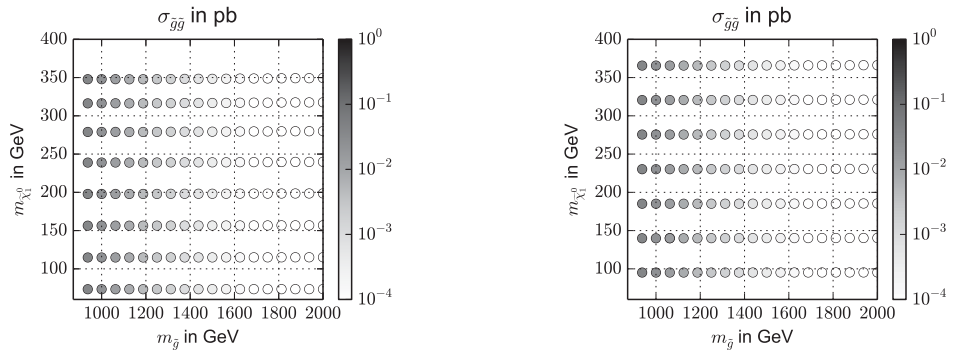

FIG. 14. Total production cross section for gluinos, using $m_{\tilde{t}_1} = 500$ GeV, $m_{\tilde{\chi}_1^\pm} = 400$ GeV. Left: λ_L. Right: λ_S.

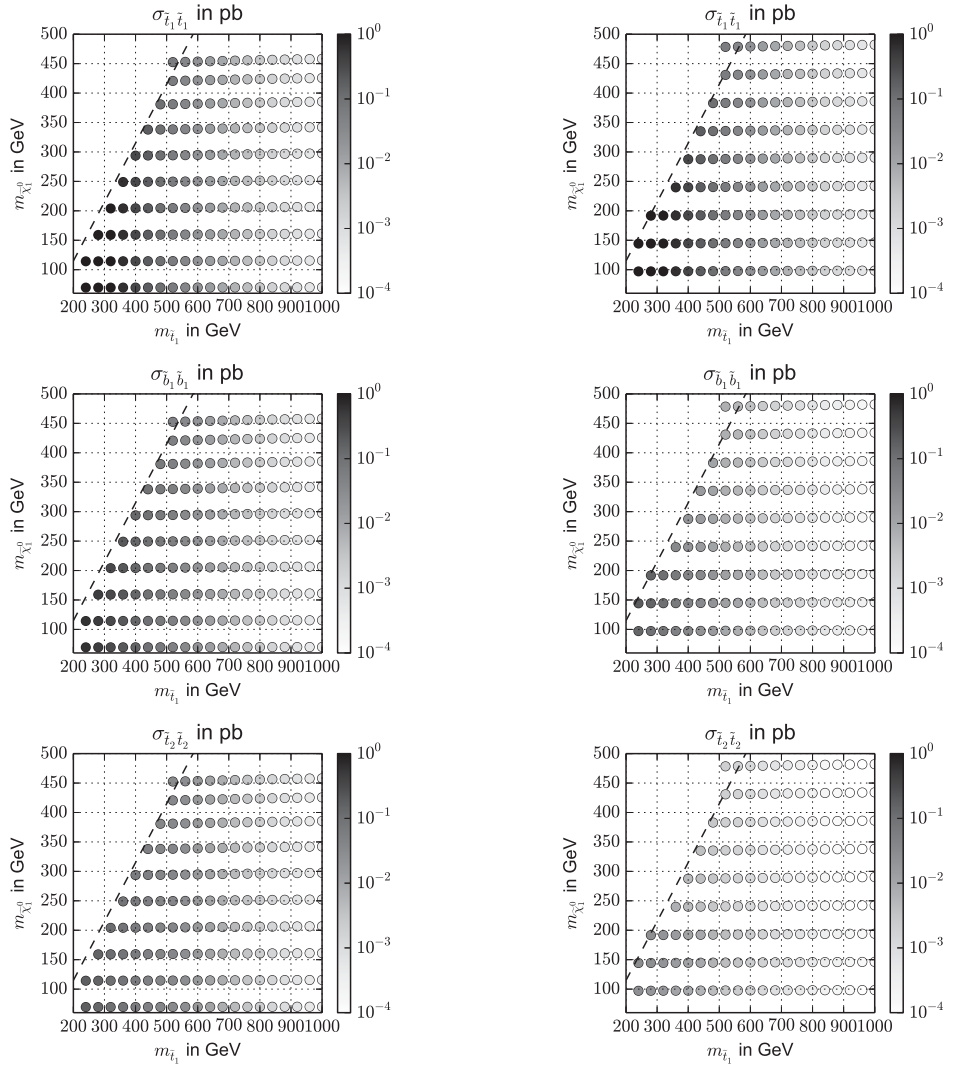

FIG. 15. Total production cross section for the third generation squarks for a decoupled gluino and $m_{\tilde{\chi}_1^\pm} = 500$ GeV. Left: λ_L. Right: λ_S

APPENDIX C: $\tilde{t}_1$ BRANCHING-RATIO DISTRIBUTIONS

An exhaustive list of plots showing distributions of branching-ratios.

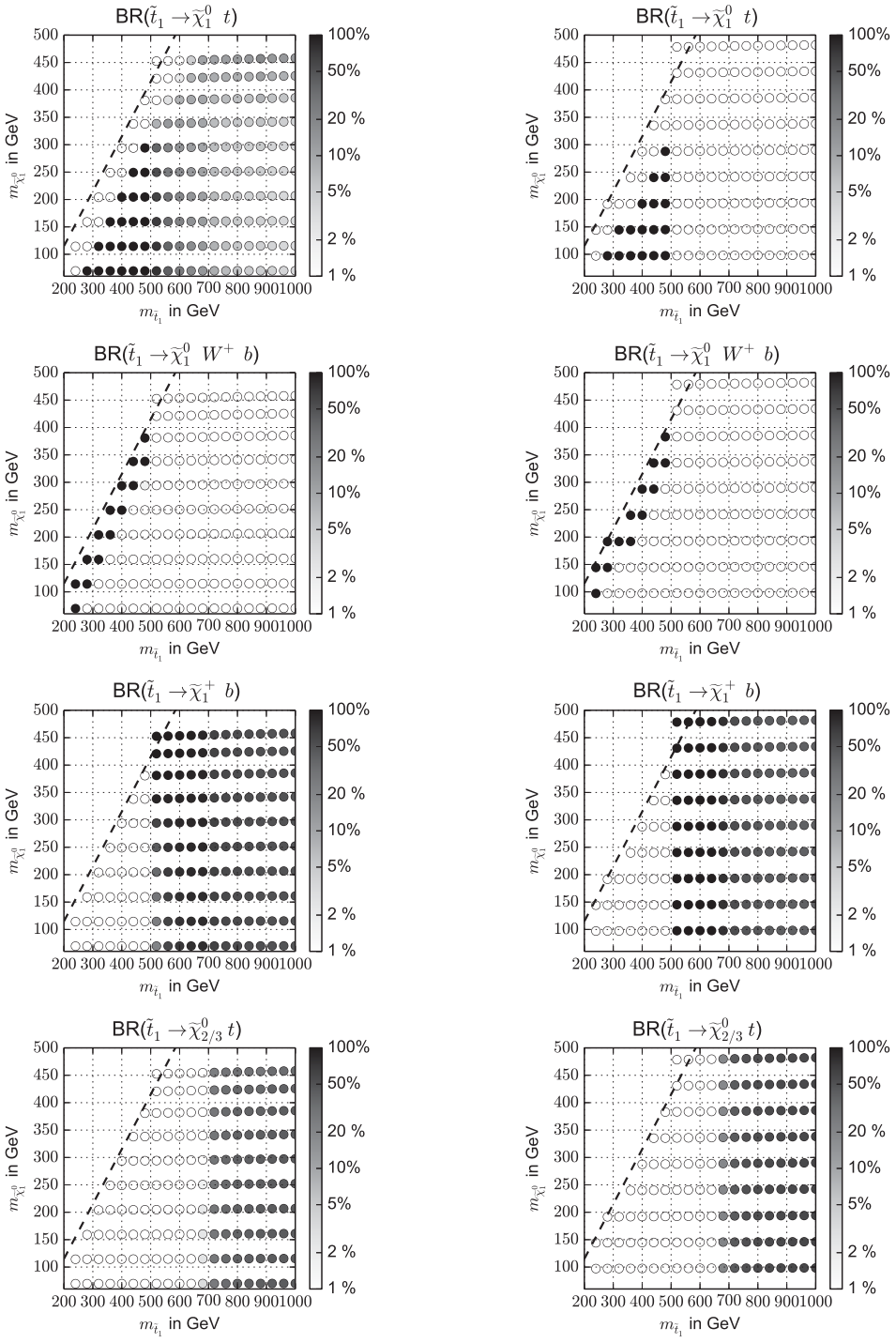

FIG. 16. Most significant branching ratios of the lightest stop into the singlino LSP, the Higgsino NLSPs and the chargino for a decoupled gluino and $m_{\widetilde{\chi}_1^\pm} = 500$ GeV. Left: λ_L. Right: λ_S

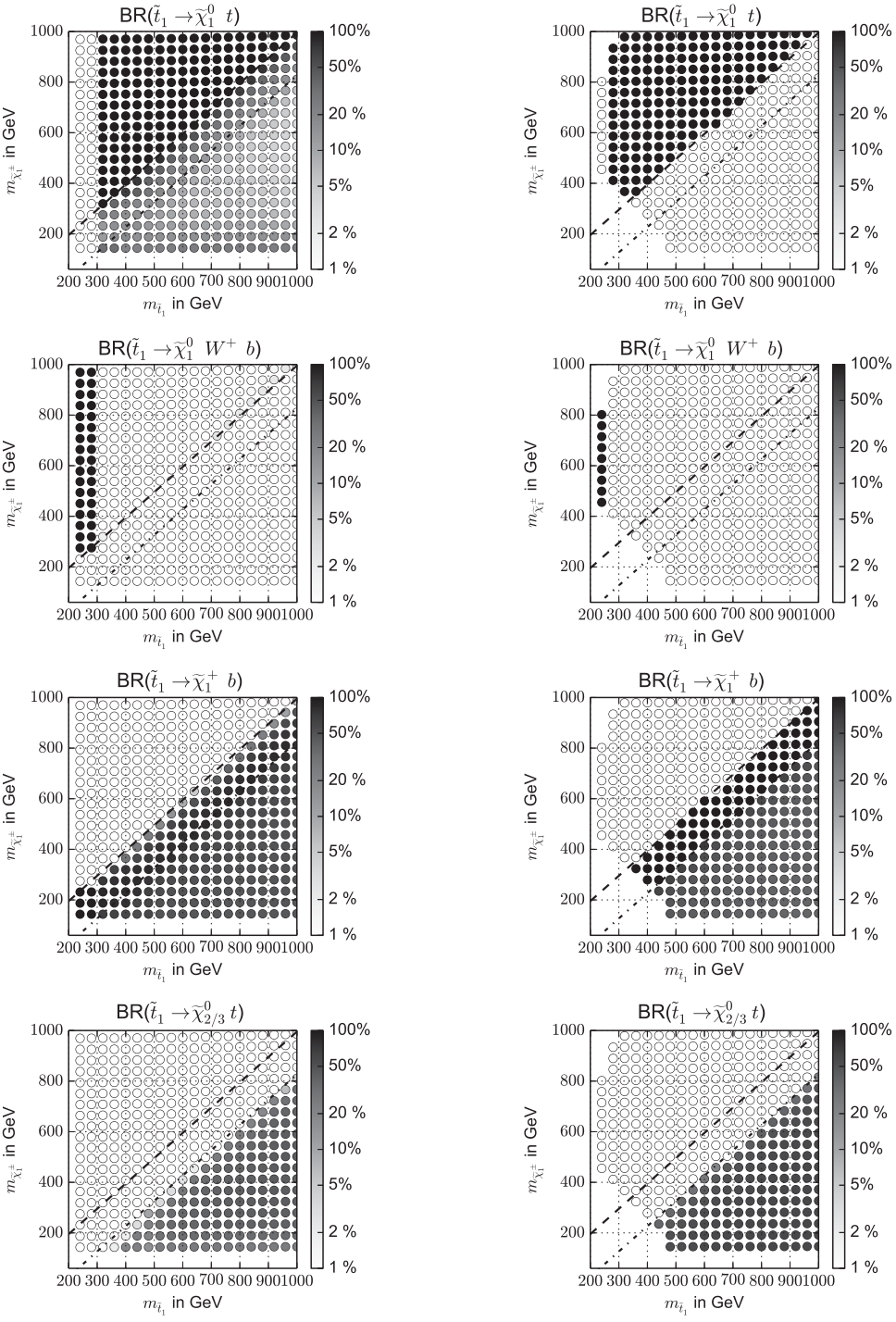

FIG. 17. Most significant branching ratios of the lightest stop into the singlino LSP, the Higgsino NLSPs and the chargino for a decoupled gluino and $m_{\tilde{\chi}_1^0} = 100$ GeV. Left: λ_L. Right: λ_S

APPENDIX D: $\tilde{b}_{1/2}$ BRANCHING-RATIO DISTRIBUTIONS

An exhaustive list of plots showing distributions of branching ratios.

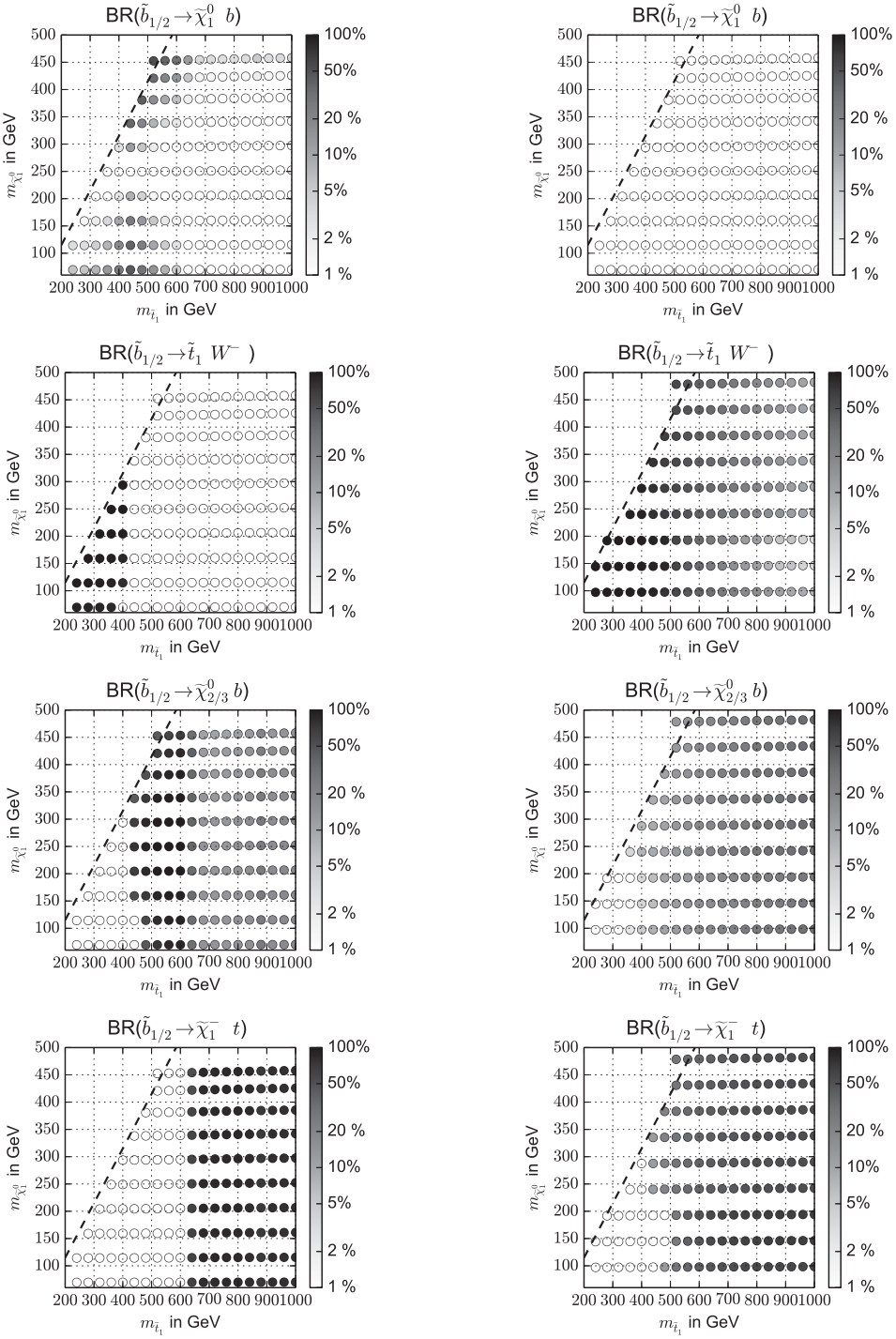

FIG. 18. Most significant branching ratios of the (mostly degenerate) sbottoms into the lightest stop, the Higgsino NLSPs and the chargino for a decoupled gluino and $m_{\widetilde{\chi}_1^\pm} = 500$ GeV. Left: λ_L. Right: λ_S

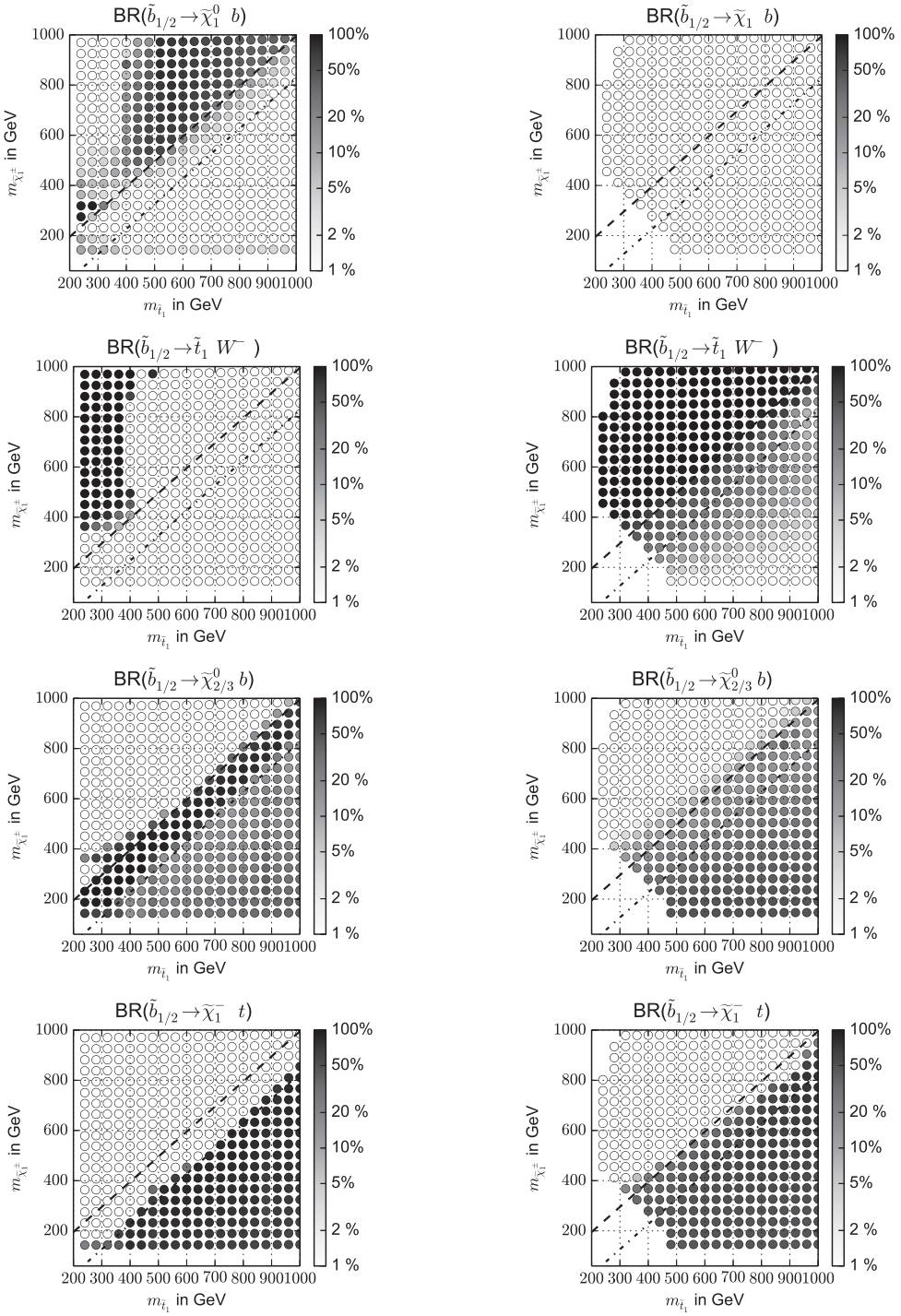

FIG. 19. Most significant branching ratios of the (mostly degenerate) sbottoms into the lightest stop, the Higgsino NLSPs and the chargino for a decoupled gluino and $m_{\tilde{\chi}_1^0} = 100$ GeV. Left: λ_L. Right: λ_S

APPENDIX E: $\tilde{t}_2$ BRANCHING-RATIO DISTRIBUTIONS

An exhaustive list of plots showing distributions of branching ratios.

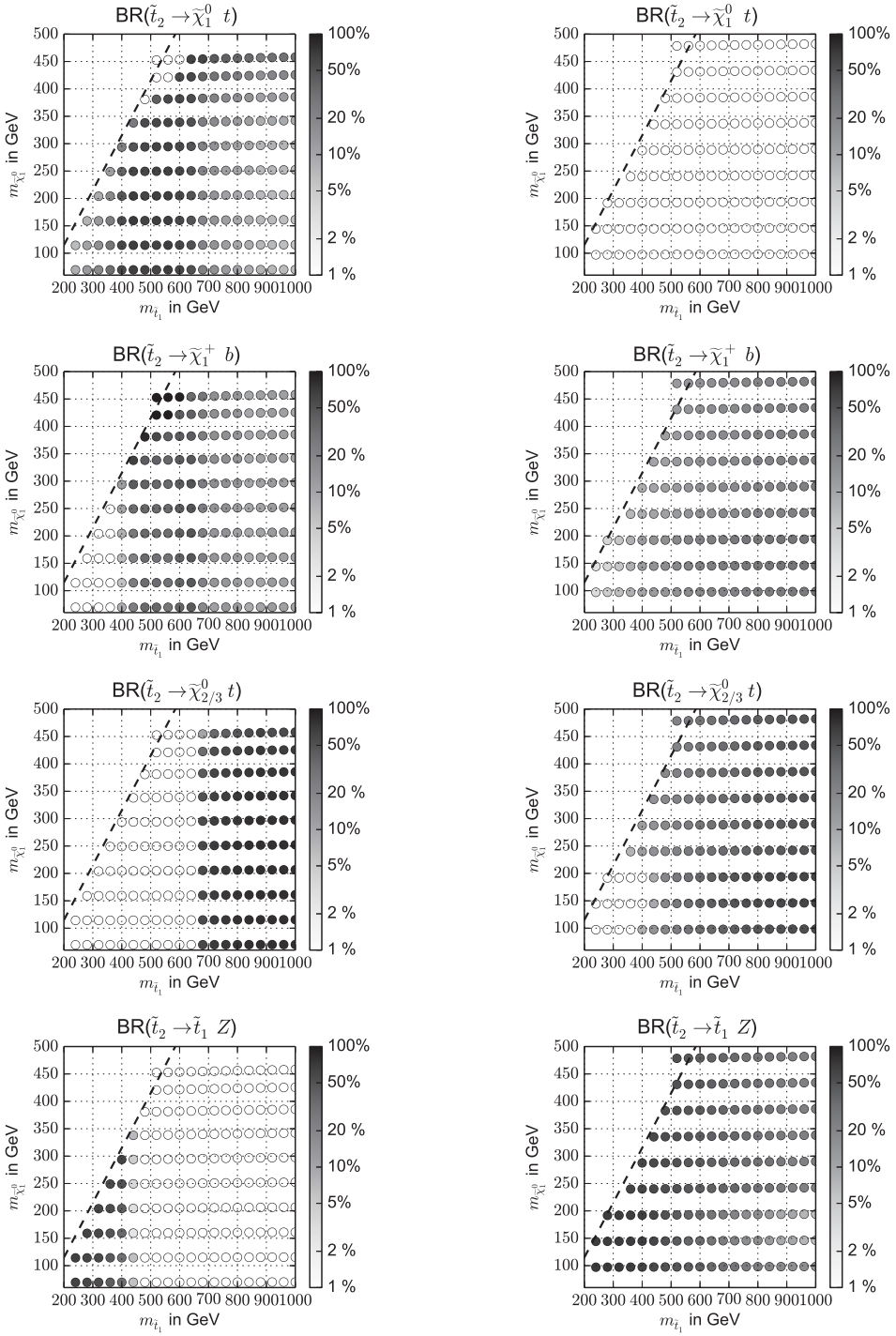

FIG. 20. Most significant branching ratios of the heavier stop into the singlino LSP, the Higgsino NLSPs and the chargino for a decoupled gluino and $m_{\widetilde{\chi}_1^\pm} = 500$ GeV. Left: λ_L. Right: λ_S

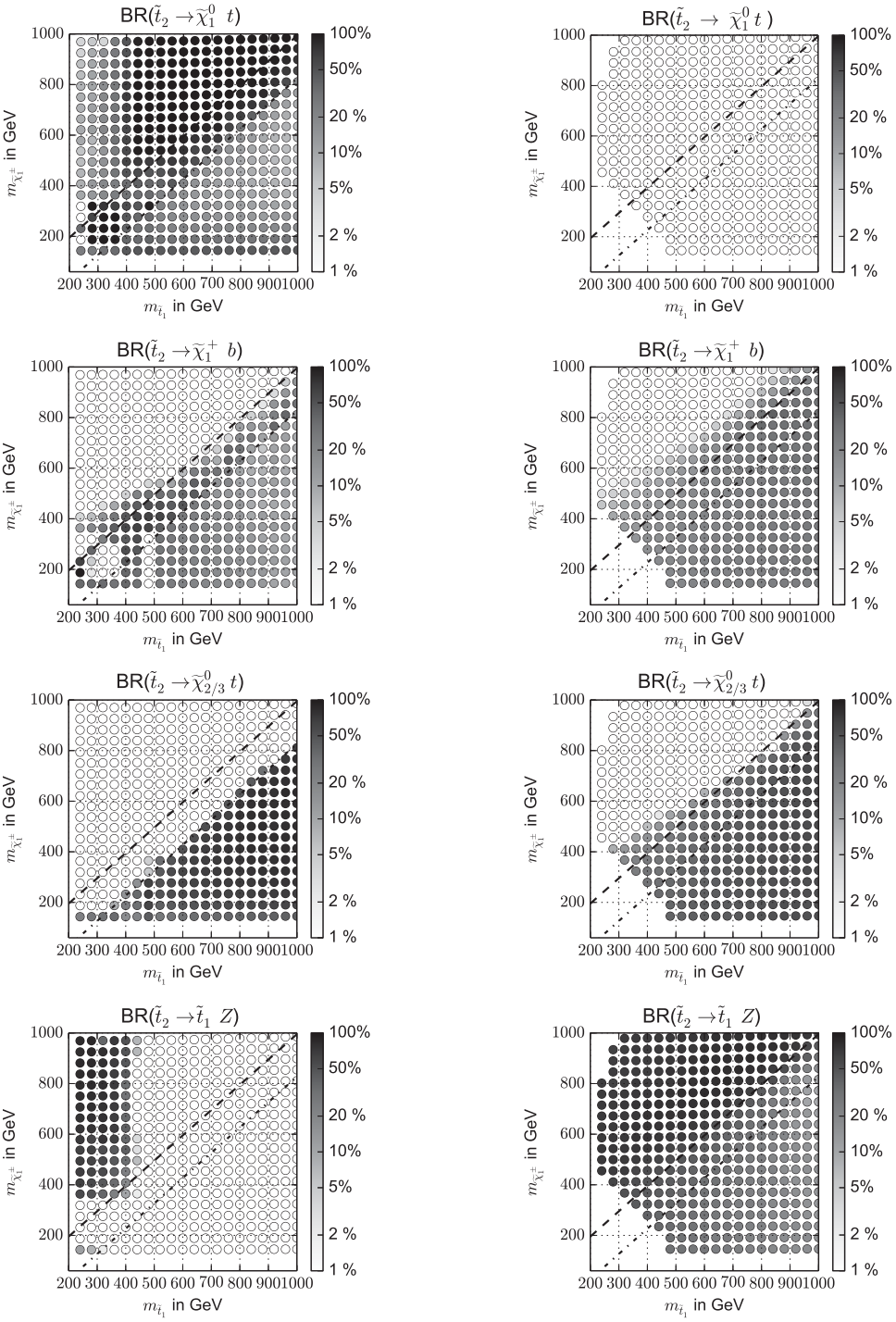

FIG. 21. Most significant branching ratios of the heavier stop into the singlino LSP, the Higgsino NLSPs and the chargino for a decoupled gluino and $m_{\widetilde{\chi}_1^0} = 100$ GeV. Left: λ_L. Right: λ_S

APPENDIX F: $\tilde{\chi}^0_{2/3}$ BRANCHING-RATIO DISTRIBUTIONS

An exhaustive list of plots showing distributions of branching ratios.

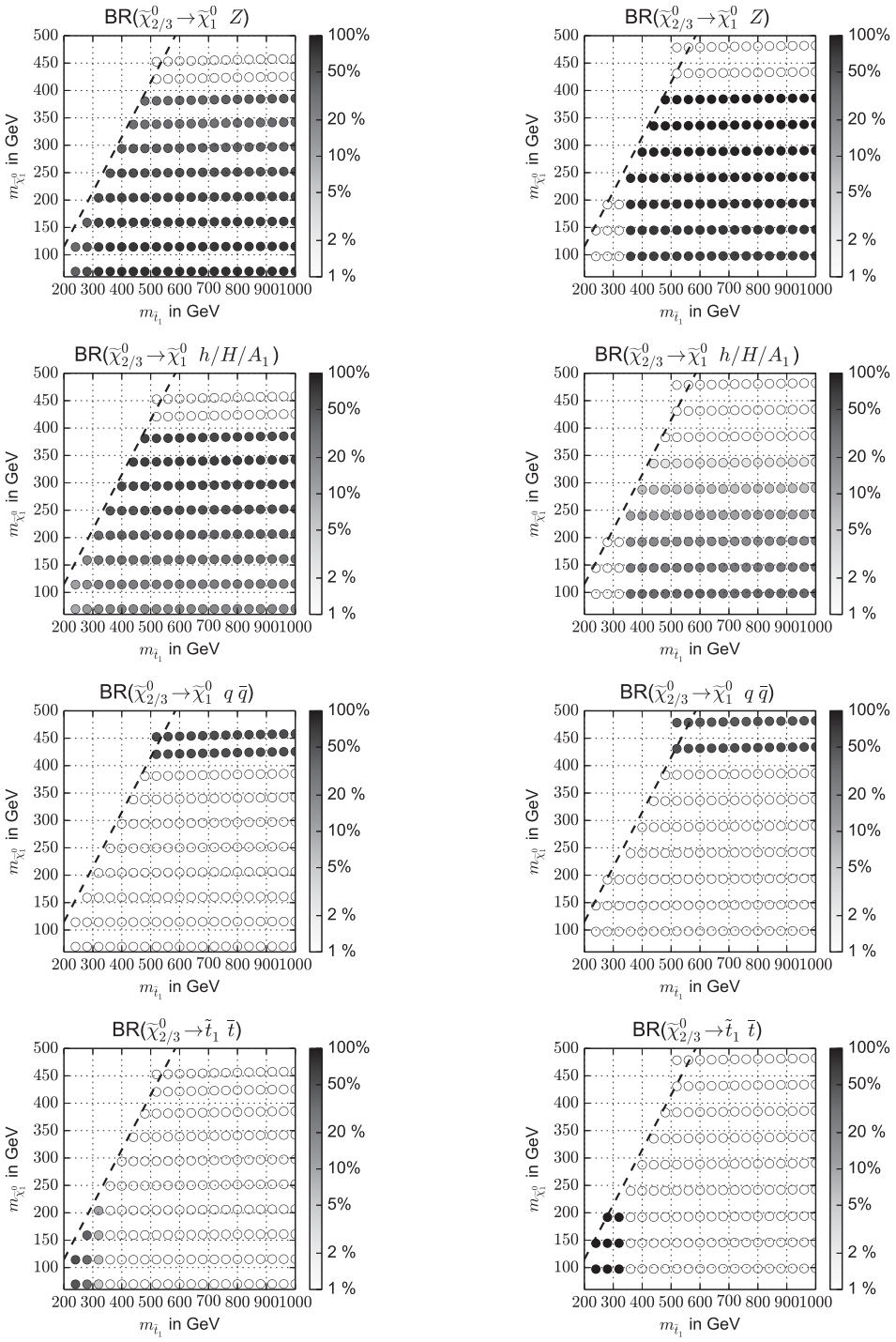

FIG. 22. Most significant branching ratios of the Higgsino-like neutralinos for a decoupled gluino and $m_{\widetilde{\chi}^\pm_1} = 500$ GeV. Left: λ_L. Right: λ_S.

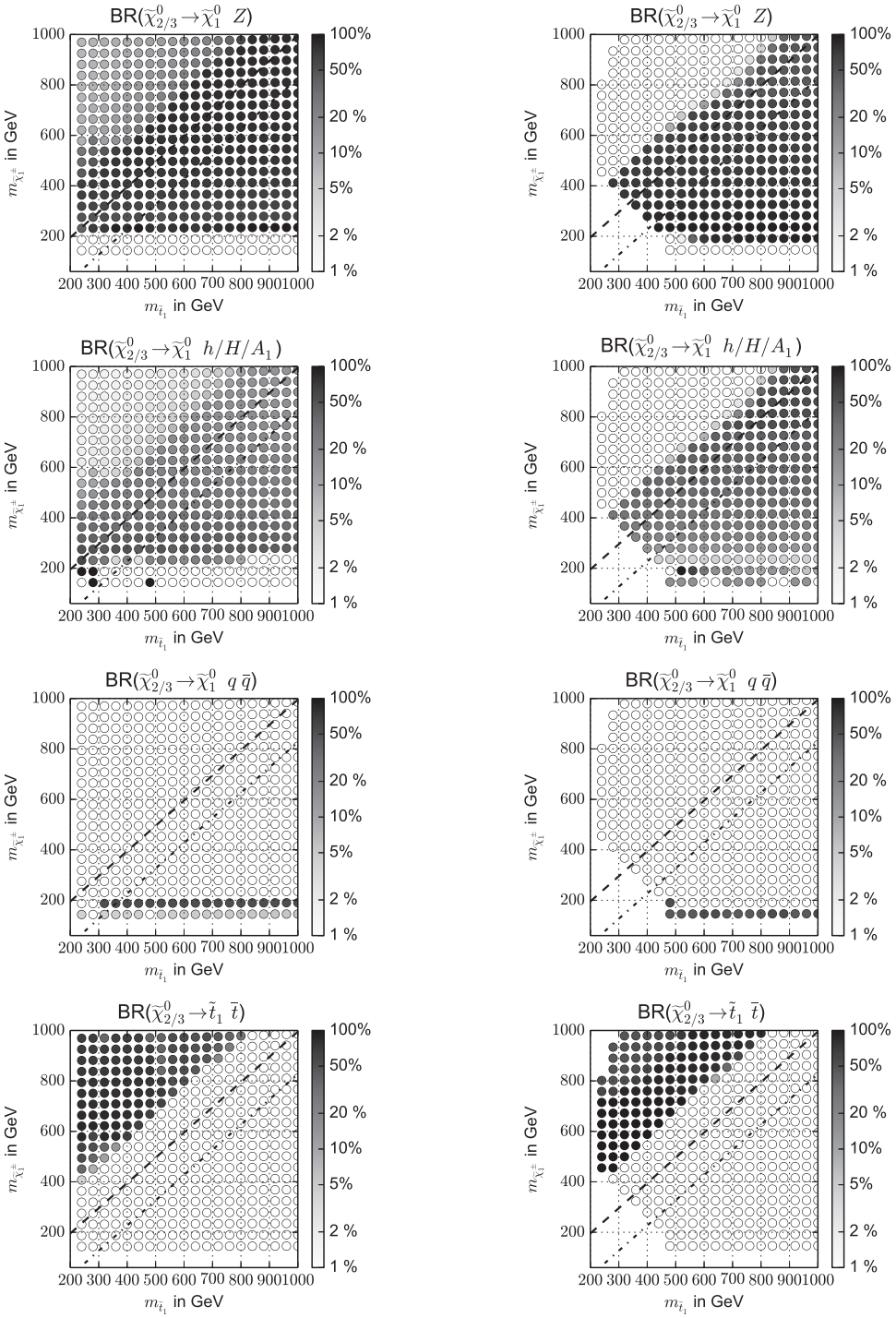

FIG. 23. Most significant branching ratios of the Higgsino-like neutralinos for a decoupled gluino and $m_{\tilde{\chi}^0_1} = 100$ GeV. Left: λ_L. Right: λ_S

[1] G. Aad *et al.* (ATLAS Collaboration), Observation of a new particle in the search for the Standard Model Higgs boson with the ATLAS detector at the LHC, Phys. Lett. B **716**, 1 (2012).

[2] S. Chatrchyan *et al.* (CMS Collaboration), Observation of a new boson at a mass of 125 GeV with the CMS experiment at the LHC, Phys. Lett. B **716**, 30 (2012).

[3] G. Aad *et al.* (ATLAS and CMS Collaborations), Combined Measurement of the Higgs Boson Mass in pp Collisions at $\sqrt{s} = 7$ and 8 TeV with the ATLAS and CMS Experiments, Phys. Rev. Lett. **114**, 191803 (2015).

[4] B. W. Lee, C. Quigg, and H. B. Thacker, Weak interactions at very high energies: The role of the Higgs-boson mass, Phys. Rev. D **16**, 1519 (1977).

[5] M. Baak, M. Goebel, J. Haller, A. Hoecker, D. Ludwig, K. Moenig, M. Schott, and J. Stelzer, Updated status of the global electroweak fit and constraints on new physics, Eur. Phys. J. C **72**, 2003 (2012).

[6] J. Wess and B. Zumino, Supergauge transformations in four-dimensions, Nucl. Phys. **B70**, 39 (1974).

[7] H. P. Nilles, Supersymmetry, supergravity and particle physics, Phys. Rep. **110**, 1 (1984).

[8] M. Drees, An introduction to supersymmetry, arXiv:hep-ph/9611409.

[9] S. P. Martin, A supersymmetry primer, Adv. Ser. Dir. High Energy Phys. **18**, 1 (1998).

[10] G. Degrassi, S. Heinemeyer, W. Hollik, P. Slavich, and G. Weiglein, Towards high precision predictions for the MSSM Higgs sector, Eur. Phys. J. C **28**, 133 (2003).

[11] P. Bechtle, S. Heinemeyer, O. Stal, T. Stefaniak, G. Weiglein, and L. Zeune, MSSM Interpretations of the LHC Discovery: Light or Heavy Higgs?, Eur. Phys. J. C **73**, 2354 (2013).

[12] L. Giusti, A. Romanino, and A. Strumia, Natural ranges of supersymmetric signals, Nucl. Phys. **B550**, 3 (1999).

[13] U. Ellwanger, C. Hugonie, and A. M. Teixeira, The next-to-minimal supersymmetric standard model, Phys. Rep. **496**, 1 (2010).

[14] J. E. Kim and H. P. Nilles, The μ problem and the strong CP problem, Phys. Lett. **138B**, 150 (1984).

[15] G. Aad *et al.* (ATLAS Collaboration), Summary of the searches for squarks and gluinos using $\sqrt{s} = 8$ TeV pp collisions with the ATLAS experiment at the LHC, J. High Energy Phys. 10 (2015) 054.

[16] M. Papucci, J. T. Ruderman, and A. Weiler, Natural SUSY endures, J. High Energy Phys. 09 (2012) 035.

[17] S. Chatrchyan *et al.* (CMS Collaboration), Search for supersymmetry in pp collisions at $\sqrt{s} = 8$ TeV in events with a single lepton, large jet multiplicity, and multiple b jets, Phys. Lett. B **733**, 328 (2014).

[18] V. Khachatryan *et al.* (CMS Collaboration), Searches for supersymmetry using the M_T2 variable in hadronic events produced in pp collisions at 8 TeV, J. High Energy Phys. 05 (2015) 078.

[19] CMS Collaboration, Report No. CMS-PAS-SUS-14-011.

[20] H. K. Dreiner, M. Kramer, and J. Tattersall, How low can SUSY go? Matching, monojets and compressed spectra, Europhys. Lett. **99**, 61001 (2012).

[21] H. Dreiner, M. Kramer, and J. Tattersall, Exploring QCD uncertainties when setting limits on compressed supersymmetric spectra, Phys. Rev. D **87**, 035006 (2013).

[22] G. Aad *et al.* (ATLAS Collaboration), Search for pair-produced third-generation squarks decaying via charm quarks or in compressed supersymmetric scenarios in pp collisions at $\sqrt{s} = 8$ TeV with the ATLAS detector, Phys. Rev. D **90**, 052008 (2014).

[23] G. Aad *et al.* (ATLAS Collaboration), ATLAS Run 1 searches for direct pair production of third-generation squarks at the Large Hadron Collider, Eur. Phys. J. C **75**, 510 (2015).

[24] S. Chatrchyan *et al.* (CMS Collaboration), Search for top-squark pair production in the single-lepton final state in pp collisions at $\sqrt{s} = 8$ TeV, Eur. Phys. J. C **73**, 2677 (2013).

[25] CMS Collaboration, Report No. CMS-PAS-SUS-13-009.

[26] K. Rolbiecki and J. Tattersall, Refining light stop exclusion limits with W^+W^- cross sections, Phys. Lett. B **750**, 247 (2015).

[27] CMS Collaboration, Report No. CMS-PAS-SUS-13-018.

[28] CMS Collaboration, Report No. CMS-PAS-SUS-13-008.

[29] S. Chatrchyan *et al.* (CMS Collaboration), Search for new physics in events with same-sign dileptons and jets in pp collisions at $\sqrt{s} = 8$ TeV, J. High Energy Phys. 01 (2014) 163; Erratum: Search for new physics in events with same-sign dileptons and jets in pp collisions at $\sqrt{s} = 8$ TeV, J. High Energy Phys. 01 (2015) 014.

[30] U. Ellwanger and A. M. Teixeira, NMSSM with a singlino LSP: Possible challenges for searches for supersymmetry at the LHC, J. High Energy Phys. 10 (2014) 113.

[31] U. Ellwanger and A. M. Teixeira, Excessive Higgs pair production with little MET from squarks and gluinos in the NMSSM, J. High Energy Phys. 04 (2015) 172.

[32] J. Cao, L. Shang, J. M. Yang, and Y. Zhang, Explanation of the ATLAS Z-peaked excess in the NMSSM, J. High Energy Phys. 06 (2015) 152.

[33] J. Cao, L. Shang, J. M. Yang, and Y. Zhang, Explanation of the ATLAS Z-peaked excess by squark pair production in the NMSSM, J. High Energy Phys. 10 (2015) 178.

[34] U. Ellwanger, Testing the higgsino-singlino sector of the NMSSM with trileptons at the LHC, J. High Energy Phys. 11 (2013) 108.

[35] J. S. Kim and T. S. Ray, The higgsino-singlino world at the large hadron collider, Eur. Phys. J. C **75**, 40 (2015).

[36] A. Chakraborty, D. K. Ghosh, S. Mondal, S. Poddar, and D. Sengupta, Probing the NMSSM via Higgs boson signatures from stop cascade decays at the LHC, Phys. Rev. D **91**, 115018 (2015).

[37] J. Beuria, A. Chatterjee, A. Datta, and S. K. Rai, Two light stops in the NMSSM and the LHC, J. High Energy Phys. 09 (2015) 073.

[38] T. Cheng, J. Li, T. Li, and Q.-S. Yan, Natural NMSSM confronting with the LHC7-8, Phys. Rev. D **89**, 015015 (2014).

[39] R. Dermisek and J. F. Gunion, Escaping the Large Fine-Tuning and Little Hierarchy Problems in the Next to Minimal Supersymmetric Model and $h \to aa$ Decays, Phys. Rev. Lett. **95**, 041801 (2005).

[40] R. Dermisek and J. F. Gunion, Next-to-minimal supersymmetric model close to the R-symmetry limit and naturalness in $h \to aa$ decays for $m_a < 2m_b$, Phys. Rev. D **75**, 075019 (2007).
[41] R. Dermisek and J. F. Gunion, Next-to-minimal supersymmetric model solution to the fine-tuning problem, precision electroweak constraints, and the largest CERN LEP Higgs event excess, Phys. Rev. D **76**, 095006 (2007).
[42] J. F. Gunion, A light CP-odd Higgs boson and the muon anomalous magnetic moment, J. High Energy Phys. 08 (2009) 032.
[43] F. Domingo, U. Ellwanger, and M.-A. Sanchis-Lozano, Bottomoniom Spectroscopy with Mixing of η_b States and a Light CP-Odd Higgs Boson, Phys. Rev. Lett. **103**, 111802 (2009).
[44] C. T. Potter, Natural NMSSM with a light pseudoscalar Higgs and singlino LSP, Eur. Phys. J. C **76**, 44 (2016).
[45] H. Dreiner, F. Staub, and A. Vicente, General NMSSM signatures at the LHC, Phys. Rev. D **87**, 035009 (2013).
[46] G. Moortgat-Pick, S. Porto, and K. Rolbiecki, Neutralinos betray their singlino nature at the ILC, J. High Energy Phys. 09 (2014) 002.
[47] G. Aad *et al.* (ATLAS Collaboration), Measurement of Spin Correlation in Top-Antitop Quark Events and Search for Top Squark Pair Production in pp Collisions at $\sqrt{s} = 8$ TeV using the ATLAS detector, Phys. Rev. Lett. **114**, 142001 (2015).
[48] G. Aad *et al.* (ATLAS Collaboration), Search for top squark pair production in final states with one isolated lepton, jets, and missing transverse momentum in $\sqrt{s} = 8$ TeV pp collisions with the ATLAS detector, J. High Energy Phys. 11 (2014) 118.
[49] ATLAS Collaboration, Report Nos. ATLAS-CONF-2013-024, ATLAS-COM-CONF-2013-011.
[50] V. Khachatryan *et al.* (CMS Collaboration), Searches for third generation squark production in fully hadronic final states in proton-proton collisions at $\sqrt{s} = 8$ TeV, J. High Energy Phys. 06 (2015) 116.
[51] G. Aad *et al.* (ATLAS Collaboration), Search for direct pair production of a chargino and a neutralino decaying to the 125 GeV Higgs boson in $\sqrt{s} = 8$ TeV pp collisions with the ATLAS detector, Eur. Phys. J. C **75**, 208 (2015).
[52] ATLAS Collaboration, Report Nos. ATLAS-CONF-2013-061, ATLAS-COM-CONF-2013-071.
[53] V. Khachatryan *et al.* (CMS Collaboration), Searches for electroweak neutralino and chargino production in channels with Higgs, Z, and W bosons in pp collisions at 8 TeV, Phys. Rev. D **90**, 092007 (2014).
[54] V. Khachatryan *et al.* (CMS Collaboration), Search for top-squark pairs decaying into Higgs or Z bosons in pp collisions at $\sqrt{s} = 8$ TeV, Phys. Lett. B **736**, 371 (2014).
[55] V. Khachatryan *et al.* (CMS Collaboration), Search for supersymmetry using razor variables in events with b-tagged jets in pp collisions at $\sqrt{s} = 8$ TeV, Phys. Rev. D **91**, 052018 (2015).
[56] M. Drees, H. Dreiner, D. Schmeier, J. Tattersall, and J. S. Kim, CheckMATE: Confronting your favourite new physics model with LHC data, Comput. Phys. Commun. **187**, 227 (2015).
[57] J. S. Kim, D. Schmeier, J. Tattersall, and K. Rolbiecki, A framework to create customised LHC analyses within CheckMATE, Comput. Phys. Commun. **196**, 535 (2015).
[58] U. Ellwanger, J. F. Gunion, and C. Hugonie, NMHDECAY: A Fortran code for the Higgs masses, couplings and decay widths in the NMSSM, J. High Energy Phys. 02 (2005) 066.
[59] U. Ellwanger and C. Hugonie, NMHDECAY 2.0: An updated program for sparticle masses, Higgs masses, couplings and decay widths in the NMSSM, Comput. Phys. Commun. **175**, 290 (2006).
[60] U. Ellwanger and C. Hugonie, NMSPEC: A Fortran code for the sparticle and Higgs masses in the NMSSM with GUT scale boundary conditions, Comput. Phys. Commun. **177**, 399 (2007).
[61] D. Das, U. Ellwanger, and A. M. Teixeira, NMSDECAY: A Fortran code for supersymmetric particle decays in the next-to-minimal supersymmetric standard model, Comput. Phys. Commun. **183**, 774 (2012).
[62] M. Muhlleitner, A. Djouadi, and Y. Mambrini, SDECAY: A Fortran code for the decays of the supersymmetric particles in the MSSM, Comput. Phys. Commun. **168**, 46 (2005).
[63] P. Bechtle, S. Heinemeyer, O. Stl, T. Stefaniak, and G. Weiglein, HiggsSignals: Confronting arbitrary Higgs sectors with measurements at the Tevatron and the LHC, Eur. Phys. J. C **74**, 2711 (2014).
[64] P. Bechtle, O. Brein, S. Heinemeyer, O. Stl, T. Stefaniak, G. Weiglein, and K. E. Williams, HiggsBounds-4: Improved Tests of Extended Higgs Sectors against Exclusion Bounds from LEP, the Tevatron and the LHC, Eur. Phys. J. C **74**, 2693 (2014).
[65] U. Ellwanger, M. Rausch de Traubenberg, and C. A. Savoy, Phenomenology of supersymmetric models with a singlet, Nucl. Phys. **B492**, 21 (1997).
[66] H. Baer, V. Barger, and D. Mickelson, How conventional measures overestimate electroweak fine-tuning in supersymmetric theory, Phys. Rev. D **88**, 095013 (2013).
[67] S. Kraml and W. Porod, Sfermion decays into singlets and singlinos in the NMSSM, Phys. Lett. B **626**, 175 (2005).
[68] U. Ellwanger and C. Hugonie, The upper bound on the lightest Higgs mass in the NMSSM revisited, Mod. Phys. Lett. A **22**, 1581 (2007).
[69] F. Staub, P. Athron, U. Ellwanger, R. Grober, M. Muhlleitner, P. Slavich, and A. Voigt, Higgs mass predictions of public NMSSM spectrum generators, arXiv:1507.05093.
[70] W. Beenakker, R. Hopker, M. Spira, and P. Zerwas, Squark and gluino production at hadron colliders, Nucl. Phys. **B492**, 51 (1997).
[71] W. Beenakker, M. Kramer, T. Plehn, M. Spira, and P. Zerwas, Stop production at hadron colliders, Nucl. Phys. **B515**, 3 (1998).
[72] A. Kulesza and L. Motyka, Threshold Resummation for Squark-Antisquark and Gluino-Pair Production at the LHC, Phys. Rev. Lett. **102**, 111802 (2009).
[73] A. Kulesza and L. Motyka, Soft gluon resummation for the production of gluino-gluino and squark-antisquark pairs at the LHC, Phys. Rev. D **80**, 095004 (2009).
[74] W. Beenakker, S. Brensing, M. Kramer, A. Kulesza, E. Laenen and I. Niessen, Soft-gluon resummation for squark and gluino hadroproduction, J. High Energy Phys. 12 (2009) 041.

[75] W. Beenakker, S. Brensing, M. Kramer, A. Kulesza, E. Laenen and I. Niessen, Supersymmetric top and bottom squark production at hadron colliders, J. High Energy Phys. 08 (2010) 098.

[76] W. Beenakker, S. Brensing, M. Kramer, A. Kulesza, E. Laenen, L. Motyka and I. Niessen, Squark and gluino hadroproduction, Int. J. Mod. Phys. A **26**, 2637 (2011).

[77] P. M. Nadolsky, H.-L. Lai, Q.-H. Cao, J. Huston, J. Pumplin, D. Stump, W.-K. Tung, and C. P. Yuan, Implications of CTEQ global analysis for collider observables, Phys. Rev. D **78**, 013004 (2008).

[78] M. Bahr, S. Gieseke, M. Gigg, D. Grellscheid, K. Hamilton *et al.*, Herwig++ physics and manual, Eur. Phys. J. C **58**, 639 (2008).

[79] J. Bellm, S. Gieseke, D. Grellscheid, A. Papaefstathiou, S. Platzer *et al.*, Herwig++ 2.7 release note, arXiv: 1310.6877.

[80] J. de Favereau, C. Delaere, P. Demin, A. Giammanco, V. Lemaître, A. Mertens, and M. Selvaggi (DELPHES 3 Collaboration), DELPHES 3: A modular framework for fast simulation of a generic collider experiment, J. High Energy Phys. 02 (2014) 057.

[81] M. Cacciari and G. P. Salam, Dispelling the N^3 myth for the k_t jet-finder, Phys. Lett. B **641**, 57 (2006).

[82] M. Cacciari, G. P. Salam, and G. Soyez, The anti-k_t jet clustering algorithm, J. High Energy Phys. 04 (2008) 063.

[83] M. Cacciari, G. P. Salam, and G. Soyez, FastJet user manual, Eur. Phys. J. C **72**, 1896 (2012).

[84] A. L. Read, Presentation of search results: The cl's technique, J. Phys. G **28**, 2693 (2002).

[85] ATLAS Collaboration, Report Nos. ATLAS-CONF-2013-062, ATLAS-COM-CONF-2013-039.

[86] G. Aad *et al.* (ATLAS Collaboration), Search for direct third-generation squark pair production in final states with missing transverse momentum and two b-jets in $\sqrt{s} = 8$ TeV pp collisions with the ATLAS detector, J. High Energy Phys. 10 (2013) 189.

[87] G. Aad *et al.* (ATLAS Collaboration), Search for direct top-squark pair production in final states with two leptons in pp collisions at $\sqrt{s} = 8$ TeV with the ATLAS detector, J. High Energy Phys. 06 (2014) 124.

[88] G. Aad *et al.* (ATLAS Collaboration), Search for supersymmetry at $\sqrt{s} = 8$ TeV in final states with jets and two same-sign leptons or three leptons with the ATLAS detector, J. High Energy Phys. 06 (2014) 035.

[89] G. Aad *et al.* (ATLAS Collaboration), Search for squarks and gluinos with the ATLAS detector in final states with jets and missing transverse momentum using $\sqrt{s} = 8$ TeV proton-proton collision data, J. High Energy Phys. 09 (2014) 176.

[90] S. Chatrchyan *et al.* (CMS Collaboration), Search for new physics in the multijet and missing transverse momentum final state in proton-proton collisions at $\sqrt{s} = 8$ TeV, J. High Energy Phys. 06 (2014) 055.

[91] J. Fan, M. Reece, and J. T. Ruderman, A stealth supersymmetry sampler, J. High Energy Phys. 07 (2012) 196.

[92] K. Rolbiecki, J. Tattersall, and G. Moortgat-Pick, Towards measuring the stop mixing angle at the LHC, Eur. Phys. J. C **71**, 1517 (2011).

[93] G. Brooijmans *et al.*, Les Houches 2013: Physics at TeV colliders: New physics working group report, arXiv:1405.1617.

[94] M. Drees, M. Hanussek, and J. S. Kim, Light stop searches at the LHC with monojet events, Phys. Rev. D **86**, 035024 (2012).

[95] S. Bornhauser, M. Drees, S. Grab, and J. S. Kim, Light stop searches at the LHC in events with two b jets and missing energy, Phys. Rev. D **83**, 035008 (2011).